Hindawi
Journal of Analytical Methods in Chemistry
Volume 2018, Article ID 1292954, 20 pages
https://doi.org/10.1155/2018/1292954

Research Article

High-Precision In Situ $^{87}Sr/^{86}Sr$ Analyses through Microsampling on Solid Samples: Applications to Earth and Life Sciences

Sara Di Salvo,[1] Eleonora Braschi,[2] Martina Casalini,[1] Sara Marchionni,[1] Teresa Adani,[1] Maurizio Ulivi,[1] Andrea Orlando,[2] Simone Tommasini,[1] Riccardo Avanzinelli,[1,2] Paul P. A. Mazza,[1] Sandro Conticelli,[1,2] and Lorella Francalanci[1,2]

[1]*Dipartimento di Scienze della Terra, Università degli Studi di Firenze, via Giorgio La Pira 4, 50121 Firenze, Italy*
[2]*C.N.R., Istituto Geoscienze e Georisorse, U.O. di Firenze, via Giorgio La Pira 4, 50121 Firenze, Italy*

Correspondence should be addressed to Eleonora Braschi; eleonora.braschi@igg.cnr.it

Received 15 December 2017; Accepted 18 February 2018; Published 22 April 2018

Academic Editor: Veronica Termopoli

An analytical protocol for high-precision, in situ microscale isotopic investigations is presented here, which combines the use of a high-performing mechanical microsampling device and high-precision TIMS measurements on micro-Sr samples, allowing for excellent results both in accuracy and precision. The present paper is a detailed methodological description of the whole analytical procedure from sampling to elemental purification and Sr-isotope measurements. The method offers the potential to attain isotope data at the microscale on a wide range of solid materials with the use of minimally invasive sampling. In addition, we present three significant case studies for geological and life sciences, as examples of the various applications of microscale $^{87}Sr/^{86}Sr$ isotope ratios, concerning (i) the pre-eruptive mechanisms triggering recent eruptions at Nisyros volcano (Greece), (ii) the dynamics involved with the initial magma ascent during Eyjafjallajökull volcano's (Iceland) 2010 eruption, which are usually related to the precursory signals of the eruption, and (iii) the environmental context of a MIS 3 cave bear, *Ursus spelaeus*. The studied cases show the robustness of the methods, which can be also be applied in other areas, such as cultural heritage, archaeology, petrology, and forensic sciences.

1. Introduction

In situ radiogenic isotope determinations with microscale resolution, especially of Sr, can represent a powerful tool in different fields of geological and life sciences. In particular, this technique is nowadays one of the most important methods for the investigation and interpretation of magmatic processes, as well as of environmentally-induced responses of terrestrial mammals; it has the potential to greatly enhance our understanding of not only volcanic systems and the related magma genesis and evolution, but also of the physiological mechanisms behind specific organic adaptations.

In situ $^{87}Sr/^{86}Sr$ provides significant data on the (i) source heterogeneities of magmas, (ii) crystallization histories within shallow level magmatic reservoirs, and (iii) magma residence times prior to eruptions (e.g., [1–10]). Since crystals record changes occurring in the environment in which they grow (e.g., [7, 11–15]), isotopic investigations at grain and subgrain scales on rock-forming minerals provide information on mineral-whole rock equilibria that constrain the magmatic processes occurring during magma evolution (e.g., mixing, mingling, crystals recycling, crustal contamination, or metasomatism). In addition, variation of Sr-isotope composition from core to rim within the same crystal can shed light on the complex pre-eruptive history of active volcanoes. Therefore, combining micro-(small-scale) isotope data with textural and petrographic data provides significant information on crystals residence time, magma production rates, and recharge dynamics (e.g., [5–8, 16–18]).

Sr-isotopic investigation has recently gained popularity in other fields, such as archaeology, anthropology, biology, cultural heritage, environmental and food studies, forensics, life and medical sciences, and palaeontology. (e.g., [19–38]). $^{87}Sr/^{86}Sr$ on tooth enamel and bone tissues gained particular attention over the last years in life studies, archaeology, palaeontology, and forensic sciences (e.g., [39–48]). In situ analyses of $^{87}Sr/^{86}Sr$ using laser ablation and multicollector-inductively coupled plasma mass spectrometry (LA-MC-ICPMS) for tooth enamel, bones, and rocks were developed in the early new millennium but have met variable success (e.g., [49–53]). At the same time, microscale sampling through drilling and micro-Sr isotope analyses by thermal ionisation mass spectrometry (TIMS) was also developed on geological materials (e.g., [6, 18, 54]). As compared with mechanical microdrilling plus TIMS procedures, LA-MC-ICPMS has the advantage of significantly reducing the time of analyses, but at the expense of precision of the measured isotope ratio; this is generally due to smaller Sr signals and the need to correct for isobaric interferences (e.g., [16, 53]).

We present a detailed protocol for in situ sampling through microdrilling, Sr purification, and thermal ionisation mass spectrometer (TIMS) high-precision determinations of small amounts of Sr (<10 ng) in both biological and geological materials at the same error levels. In situ $^{87}Sr/^{86}Sr$ analysis is presented in three case studies which deal with the following: (i) plagioclase crystals from Nisyros volcano (Greece), (ii) glassy matrix of single glassy clasts from the 2010 eruption of the Eyjafjallajökull volcano (Iceland), and (iii) bones and teeth from fossil remains of the *Ursus spelaeus*. In these three examples, the in situ Sr-isotope approach permits to constrain petrological and volcanological processes and to effectively outline the life habits and habitat exploitation of extinct living species. The three presented cases aim to show the high potential of the methodology, validating its wide-scale applicability in many other areas, such as cultural heritage, archaeology, and forensic sciences.

2. Materials and Methods

Technological improvements on mass spectrometer and microsampling devices allow researchers to collect and analyse small amounts of sample (few micrograms of sample, containing nanograms of Sr) with no loss of precision in the isotopic determination. In situ analyses have many important advantages over more typical ones on bulk samples. In geological applications, it allows to preserve the textural information and thus to combine it with the isotopic and geochemical composition of specific portions of the samples. In archaeology and palaeontology, this method has the advantage of minimising the damage and/or destruction of samples, thereby leaving significant amounts available for further applications.

The procedure consists in three main stages: (i) in situ sampling through microdrilling, (ii) sample digestion and purification of the element of interest, in our case Sr, and (iii) measurement of the isotope ratios (i.e., $^{87}Sr/^{86}Sr$) through thermal ionisation mass spectrometry (TIMS). Our Radiogenic Isotope Laboratory at the Department of Earth Sciences of the Florence University is equipped with a modern MicroMill™ grinder device, an ultraclean laboratory ("Class 1000") for microsamples digestion and elemental separation and a thermal ionisation mass spectrometer (ThermoFinningan™ Triton-Ti®) for isotopic measurements.

Compared to classic, bulk sample analyses (generally measured on 100–150 ng of Sr [55]), small-sample analysis (typically 5 to 10 ng of Sr) has the drawback of being more exposed to contamination from Sr alien to the sample. In situ micro-Sr measurements therefore require continued testing of laboratory blanks during the whole analytical procedure.

2.1. In Situ Sampling

2.1.1. The Microdrilling Device. Microsampling on minerals, glasses, and tooth enamel reported in this paper was performed using a microdrilling device capable of high resolution milling (New Wave-Merchantek MicroMill™, https://www.esi.com/products/laser-processing/milling/micromill/). The MicroMill (Figure 1(a)) combines a binocular microscope (with 6.7x–40x magnifying power) with remotely controlled submicron stage resolution and positional accuracy and a real-time video observation (at 3x digital magnification). It includes a low-eccentricity high-torque milling chuck, with variable speed (1,200–35,000 rpm), wherein a tungsten carbide or diamond-tipped bit is fixed, and an automated high-precision sliding stage on which the sample is loaded (Figure 1). The open stage architecture can accommodate thin sections or mounts and also larger solid samples such as bones, shells, ceramics, and plastics. The plug where the bit is hosted moves with adjustable speed for both spin and vertical movement, along the Z direction. The stage moves along the X-Y direction with a precision of 1 μm and maximum shift of 5 cm, allowing a high spatial resolution to the micron scale. This yields high spatial resolution, to the micron scale, and allows small-size sampling (i.e., a few μg of powder). The digital camera, placed next to the milling chunk (Figure 1(c)), shows a live image of the stage and of the bit position (Figure 2(a)). Using the microscope position mode (scope position), the optical image of the sample can be monitored on the PC screen prior to and after the sampling (Figure 2(b)).

The device allows in situ microsampling on several types of solid materials such as rocks, minerals, glasses, plastics, bone tissues, ceramics, metals, and alloys. The designed software package also allows performing different milling patterns such as holes arranged randomly, lines, or rasters (Figure 2(b)). Fine adjustment of milling velocity helps the microsampling of solid materials with different hardness.

Microsampling on geological (e.g., rock, minerals, and glasses) and archaeological materials (glasses, ceramics, teeth, and bones) is performed using either thick polished sections (some 100 μm thick) or sample mounts (e.g., small chunks, chips, fragments of bones, and teeth). In our case studies, we used thick, polished sections for mineral and volcanic glasses and mounts for the teeth; both were fixed on the stage using either a double-sided adhesive tape or hot glue, to avoid sample displacement during milling. Thick, polished sections are preferable for geological samples because they permit to

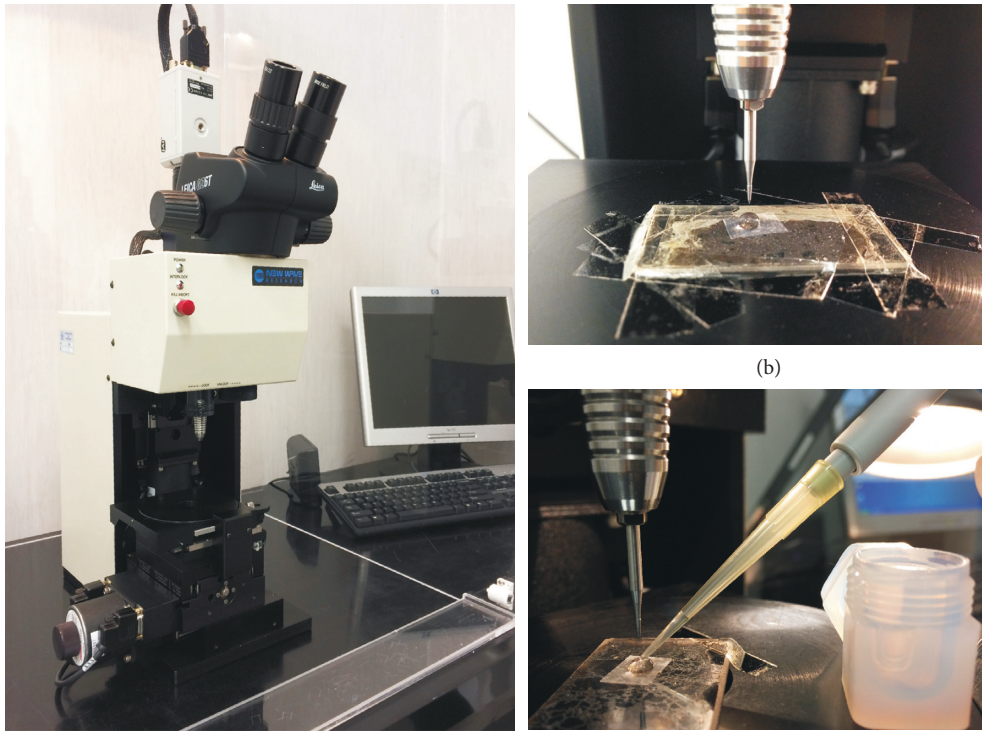

(a) (b) (c)

Figure 1: (a) The New Wave-Merchantek Micromill device operating at the Department of Earth Sciences–University of Firenze; (b) image of a petrographic polish thick section fixed on the sample stage under the tungsten carbide drilling bit that is locked into the milling chuck. A Milli-Q droplet constrained by the Parafilm is placed on the section in order to collect the powder during the drill; and (c) sample slurry recovery from the drilled surface into the digestion beaker.

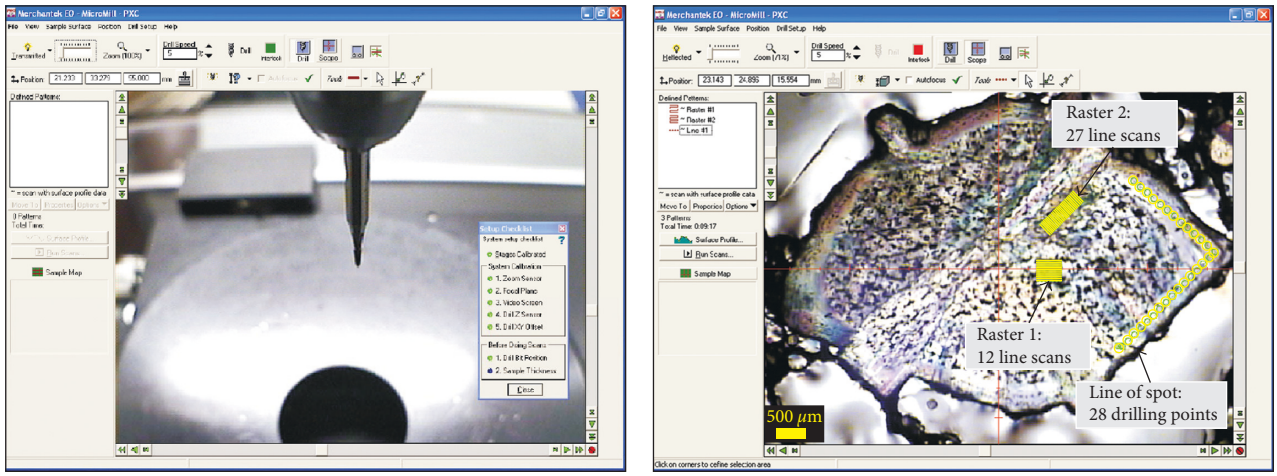

(a) (b)

Figure 2: (a) Live image of the sample stage and drill bit shown by the digital camera placed next to the milling chuck; (b) microscope view image showing a zoned plagioclase crystal with drilling pattern. Two rasters (in yellow) are set up to drill the plagioclase core, whereas a line of spot is set up for the rim microdrilling.

characterise the petrographic features of the samples and thus to perform the microsampling according to their textural properties.

2.1.2. Milling Procedure and Sample Collection. A droplet of Milli-Q® water is placed with a micrometric pipette on the selected area prior to milling; this is performed by sticking a small punched square of warmed-up Parafilm™ on the sample surface (Figure 1(c)). The water droplet retains the powder produced by the milling, which can then be easily collected by pipetting; it has also the effect of cooling the microdrill bit while milling. Before each drilling session, the drill bit is ultrasonically cleaned with pure ethanol and then rinsed with Milli-Q water.

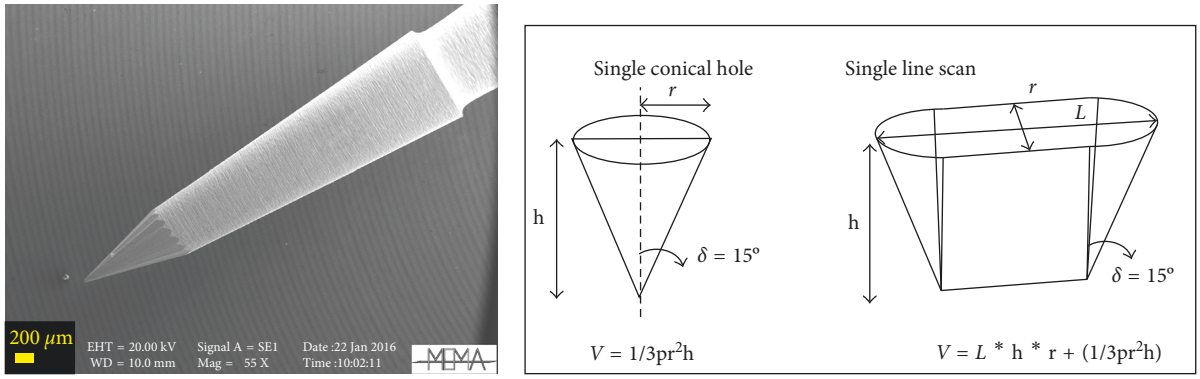

(a) (b)

Figure 3: (a) SEM imaging of a tungsten carbide drill bit used for milling: the tip angle is 30° and geometrical shape of (b) a single conical hole and single line scan.

The instrument software provides different drilling patterns and depths: single or multiple independent holes, spot lines, grids, line scans, or rasters (Figure 2(b)). Milling spot lines (or grids) are more accurate, but more time-consuming; they were used for the geological material (crystals and volcanic ashes) which requires more precise spatial resolution between the different zones of the same crystal or between the thin films of glass. Milling failure, such as crystal breaking, was prevented by setting a slow scan speed and splitting the milling into two or more steps. Line scans, which are performed faster but less accurately, were used for drilling the teeth. The number of points, lines, or rasters to be milled (which accounts for the amount of Sr to be collected) need to obtain a sufficient quantity of Sr for the TIMS measurements and can be calculated based on (i) the Sr content of the sample (independently determined by LA-ICPMS), (ii) the geometry of the drill bit, and (iii) the drilling pattern and the depth. Tips of different size and shape can be used for the drilling; therefore, the volume of material actually removed from different depths of a single hole or at different depths and lengths of a single line needs to be carefully calculated. The tungsten carbide mill bits supplied with the microdrill device (Komet–Brassler), have conical shape with an angle of 30° (Figure 3). The volume removed during each drilling is equivalent to that of the conical tip and dependent on the geometry of the drilling pattern, as well as on the specific depth (Figure 3). The minimum amount of sample that needs to be drilled depends also on the total procedural blank, which should be at least two orders of magnitude lower than the total amount of Sr collected from the sample.

After milling was completed, the sample slurry was collected with a micropipette in a PFA beaker and then transferred in the clean lab for sample digestion and elemental purification. The blanks of the milling procedure were determined by keeping the drill bit tip into a Milli-Q water droplet on the sample surface (accurately cleaned before use) for as long as the average sampling time; the droplet was then processed as an ordinary sample. The amount of Sr in the blank was then determined through isotope dilution, by adding a single-spike solution (enriched in ^{84}Sr).

2.2. Sample Dissolution and Sr Purification. The purification of the element of interest, in our case Sr, is crucial to obtain high-precision isotopic measurements for at least two reasons. First, it avoids isobaric interferences on the masses that will be analysed by mass spectrometry; in the specific case of Sr isotope measurements, even a small amount of ^{87}Rb will add to ^{87}Sr, yielding an overestimate of the ^{87}Sr/^{86}Sr ratio. Secondly, the presence of other elements of the matrix will compete with Sr during the thermal ionisation process, reducing the Sr signal and thus yielding less accurate measurements. The possibility of collecting and processing the sample for the purification of the element of interest is one of the major advantages of the method presented here over other methodologies, which do not achieve the same degree of accuracy and precision. The LA-MC-ICPMS methods allow faster data acquisition and higher sample throughput than mechanical microdrilling plus TIMS procedures, thanks to the possibility of introducing the samples directly into the mass spectrometer without chemical separation. On the other hand, LA-MC-ICPMS measurements require careful monitoring and corrections to minimize isobaric interferences in order to achieve suitable analytical accuracy and precision (e.g., [49, 53, 54, 56]).

Powder digestion and Sr purification were carried out in our ultraclean laboratory ("Class 1000") aiming at the following: (i) optimising the separation of Sr and Rb to avoid interference of ^{87}Rb with ^{87}Sr, (ii) purifying the Sr collection form all the matrix analytes, (iii) maximising the yield of the columns during the chromatographic purification, and (iv) preserving low procedural blanks. Sample digestion was performed by sequential HF-HNO_3-HCl as described in [55]. Chromatographic Sr purification was performed using Eichrom® Sr-Spec™ resins (100–150 μm) in quartz microcolumns (0.14 ml volume; Figure 4). Matrix elements were flushed out through elution with 14 column volumes of 3 N HNO_3. Sr was then collected in Milli-Q (13 column volumes). The collected Sr fractions were further treated with concentrated HNO_3 and H_2O_2 (fluxing at 150°C on a hotplate) to remove any organic residue. After this final step, samples were diluted in HNO_3 (10 vol.%) and were finally ready for loading on filaments for mass measurements. The

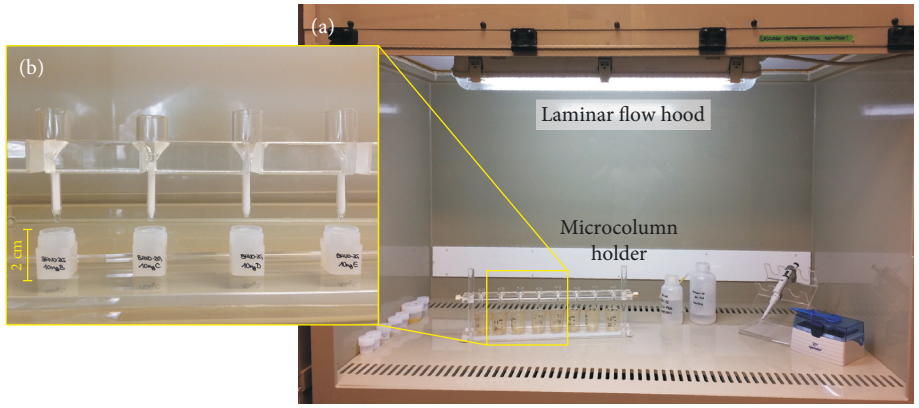

Figure 4: (a) Image of the laminar flow hood used for chemical processing and Sr separation of microdrilled samples; (b) image of quartz microcloumns filled with approximately 140 μl of specific chromatographic resin (Eichrom Sr-Spec, 100–150 μm) with high Sr-recovery efficiency, for Sr element extraction.

Table 1: Blank contamination level.

	Laboratory blanks			Isotope ratios on blanks		
Standard procedure on large size samples	Sr pg	1 SD	*n*	$^{87}Sr/^{86}Sr$	1 SD	*n*
	127	60	32	0.707497	0.000060	5
Procedure on small size samples						
Total procedure (drilling, digestion, and elemental selection)	38	19	16			
Chemical digestion and separation	17	6	12			

1 SD, standard deviation (external precision); *n*, numbers of blank measurements; the average Sr-isotope value obtained from 5 unspiked blanks is reported to fully characterize the potential contamination component.

whole analytical procedure was performed with acids of ultra-pure quality.

In order to thoroughly assess the contamination levels, we measured two types of blanks, one considering only the amount of Sr deriving from the chemical digestion and Sr separation, the other accounting for the whole procedure, including the drilling process, as described in the previous section. The results were 17 ± 6 (1 SD, $n = 12$) and 38 ± 19 pg (1 SD, $n = 16$), respectively, over a 14-month period (Table 1), thus allowing sampling as low as 4 ng of Sr for isotope analysis.

2.3. $^{87}Sr/^{86}Sr$ Measurements on TIMS. Sr isotope ratios were determined using a multicollector, thermal ionization mass spectrometer (TIMS: ThermoFinningan Triton-Ti™) (Figure 5), equipped with nine moveable collectors, which allow to simultaneously detect all the natural masses of Sr (^{84}Sr, ^{86}Sr, ^{87}Sr, and ^{88}Sr). The mass of ^{85}Rb was also measured to monitor possible ^{87}Rb interference, but it was always lower than the detection limit of the instrument, confirming the quality of the separation procedure described above. A detailed description of instrumental characteristics and performances are given in [55], along with standardised routine, measuring conditions, and setting for normal-sized samples (100–150 ng of Sr). Instrumental mass bias (e.g., [57–59]) was corrected to the natural value of $^{86}Sr/^{88}Sr = 0.1194$ using an exponential law (e.g., [55, 59]).

The most critical aspects of measuring small-size samples are related to (i) the procedure of sample loading onto the filaments and (ii) the measurement mode (i.e., static versus multidynamic, e.g., [55, 59]). Both are very important to maximise the Sr signal during the measurements, to balance the analysis time and the analytical errors that are a function of sample size.

The measurement protocol was tested by replicate analyses of an international certified standard (NIST-SRM987), properly diluted to attain sample sizes (5 to 10 ng Sr) comparable to those of the microsamples. Then, we tested the whole procedure, from in situ sampling (<10 ng of Sr) to isotope measurement, on the international glass reference sample BHVO-2G. BHVO-2G reference sample is a synthetic basaltic glass (provided by USGS) obtained by melting the BHVO-2 powder collected from a Hawaiian lava flow. The glassy slices are supplied in epoxy resin mounts (https://crustal.usgs.gov/geochemical_reference_standards/microanalytical_RM.html).

2.3.1. Sample Loading onto Filament. The Sr fraction collected from the columns was dissolved into 1 μl HNO_3 10 vol.% and loaded on single Re filaments under a horizontal laminar flow hood. Due to the small amount of Sr available, it is important to confine the sample on the smallest possible area on the filament, so that the whole loaded sample can be ionised at the same time from a single spot. To attain this, a thin layer of Parafilm™ was melted at both sides of the filament surface, to prevent any spreading of the solution, leaving a small gap (1 mm) for the droplet at the center on the filament (Figure 5(b)). The loading was performed by sandwiching the sample between two 0.5 μl

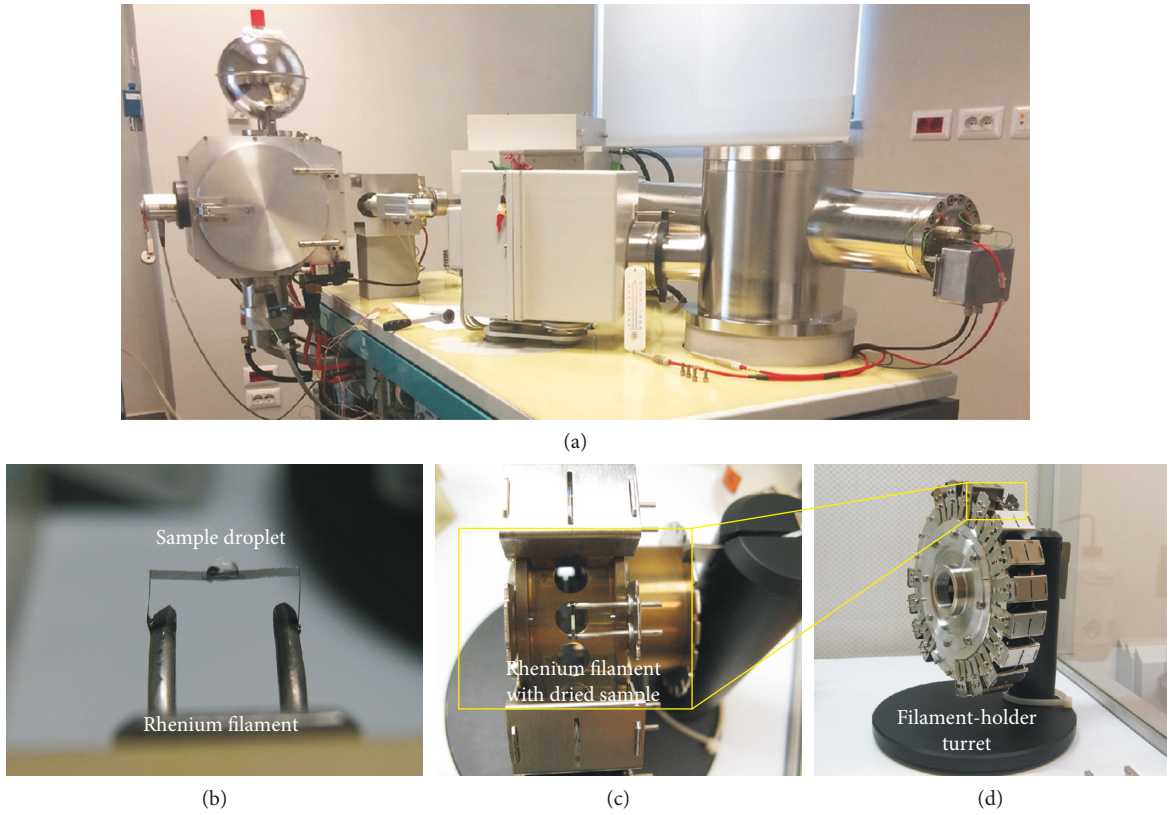

FIGURE 5: (a) The ThermoFinningan Triton-Ti multicollector, thermal ionization mass spectrometer (TIMS) at the University of Firenze; (b) single-rhenium filament with a sample droplet on top; (c) detail of a single filament, holding a dried sample loaded on a sample holder turret that can host 21 filament positions; (d) the turret is ready for the installation into the thermal ionization mass spectrometer.

drops of $TaCl_5$ activator solution [55] and 0.5 μl of H_3PO_4 solution (6 vol.%), respectively. $TaCl_5$ activator was added for enhancing Sr ionisation efficiency and H_3PO_4 for stabilising Sr isotope fractionation during measurement. All the solutions (i.e., activator, sample, and H_3PO_3) were slowly dried by passing a current on the filament, which was increased at the end of the procedure until the filament starts glowing. The loaded filaments were then placed on the filament-holder turret and then inserted into the mass spectrometer (Figures 5(c) and 5(d)).

2.3.2. Measurement Procedure Reproducibility and Accuracy. The measurement routine was established to obtain the best internal and external precisions, and the accuracy, on $^{87}Sr/^{86}Sr$, was achieved by experimentally comparing runs performed in *static* versus *dynamic* conditions at a variable number of cycles and integration times. A detailed description of the *static* and *dynamic* methods is provided in [55, 59]. In brief, the static mode consists of simultaneous measurements of all isotopes in a single "jump," so that the magnetic field remains static and the masses always hit the same detectors (Table 2). *Static* measurements have the advantage of considerably reducing the acquisition time in comparison with the *dynamic* mode, which becomes important when little amount of Sr is available, as dealing with small samples. The main limitation of this method is related to the uncertainty on the Faraday cup efficiency and on the drift of the electronics (i.e., the amplifiers). The Triton-Ti is equipped with a virtual amplifier, which enables a variable connection between amplifiers and Faraday cups and allows a complete switching between amplifiers and cups during a single measurement. However, the virtual amplifier is not able to correct for the different Faraday cup efficiency and its variation with time.

In contrast, the *dynamic* (or *multidynamic*) mode is a peak-jumping procedure where a number of different cup configurations are employed for determining a single isotopic ratio (Table 2). This means that each isotope beam is measured sequentially in different Faraday cups, so that two $^{87}Sr/^{86}Sr_{double}$ values (Table 2) can be calculated without cup efficiency biases and drifts of the electronics (Table 2). The two $^{87}Sr/^{86}Sr_{double}$ values are then geometrically averaged to obtain a single $^{87}Sr/^{86}Sr_{triple}$ value.

The best configuration for *static* mode measurements was found by measuring 300 cycles with an integration time of 8 s, which corresponds to a total measuring time of about 35 minutes for each sample. For *dynamic* mode measurements, we performed 120 cycles (each including 3 magnetic jumps), with 8 s of integration time and an idle time of 3 s between the different jumps, for a total of 70 minutes for each sample.

In both *static* and *dynamic* methods, the filament was slowly warmed up, for a total of about 45 minutes, to stabilise the ion emission until the suitable intensity is achieved. During the heating, the beam was accurately optimised by peak-centering and focusing. The optimal beam intensity for

Table 2: Cup configuration schemes of static (a) and dynamic (b) mode measurements.

Cup	L4	L3	L2	L1	C (Far)	H1	H2	H3	H4
(a) Static collection mode									
		^{84}Sr	^{85}Rb	^{86}Sr	^{87}Sr	^{88}Sr			
(b) Dynamic collection mode									
Jump 1			^{85}Rb	^{85}Rb	^{86}Sr	^{87}Sr	^{88}Sr		
Jump 2 (main)		^{84}Sr	^{86}Sr	^{86}Sr	^{87}Sr	^{88}Sr			
Jump 3				^{87}Sr	^{88}Sr				
Sr double									

Combining the measurements from two different magnetic field position (jump 1-2 and jump 2-3 above), it is possible to evaluate two independent $^{87}Sr/^{86}Sr_{double}$ defined as follows: $[^{87}Sr/^{86}Sr]_{1\text{-}2} = \sqrt{[^{87}Sr_{H1}/^{86}Sr_{C}]_1 \cdot [^{87}Sr_{C}/^{88}Sr_{H1}]_2 \cdot [^{88}Sr/^{86}Sr]_N}$ and $[^{87}Sr/^{86}Sr]_{2\text{-}3} = \sqrt{[^{87}Sr_{C}/^{86}Sr_{L1}]_2 \cdot [^{87}Sr_{L1}/^{88}Sr_{C}]_3 \cdot [^{88}Sr/^{86}Sr]_N}$. The numbers outside the parentheses are relative to the three different magnetic field positions, the subscript of each isotope refers to the cup on which it is measured, and $[^{88}Sr/^{86}Sr]_N$ is the natural ratio (i.e., 8.375209)

the measurement varied from *static* to *dynamic* mode, with higher intensity allowed by the shorter *static* (3–3.5 V on ^{88}Sr) mode with respect to *dynamic* (1.5–2 V on ^{88}Sr) mode, which instead requires maintaining a stable beam, owing to the longer duration of the measurement.

The results are shown in Figure 6 and Table 3. *Static* and *dynamic* mode measurements on NIST-SRM987 reference samples (10 ng of Sr measured) yielded $^{87}Sr/^{86}Sr$ average values of 0.710247 ± 0.000026 (2 SD, $n = 30$) and 0.710251 ± 0.000018 (2 SD, $n = 51$), respectively, with internal precisions of 13 ppm (2 SE) and 16 ppm (2 SE), respectively. Both values are within the recommended reference value for NIST-SRM987 ($^{87}Sr/^{86}Sr = 0.710248 \pm 0.000011$; Figures 6 (a) and 6(b) and Table 3 [59]). *Static* measurement reduced the experimental time but showed a worse external reproducibility than that obtained in *dynamic* mode (Figures 6(a) and 6(b)), yet maintaining similar internal precision. Therefore, the *dynamic* mode was chosen for the experimental work both on the international glass standard BHVO-2G and on the unknown samples. Further measurements of SRM987 in the *dynamic* mode were performed after the initial testing, along with the studied samples, yielding consistent results ($^{87}Sr/^{86}Sr = 0.710252 \pm 0.000018$, 2 SD, $n = 47$; Figure 6(c)).

Results on the BHVO-2G are reported in Table 3. The results were also compared to standard measurements (150 ng of Sr) on the BHVO-2 powder reference sample. BHVO-2G versus BHVO-2 results found for micro- and normal-size samples, respectively, are well within the internal analytical error (Table 3) and in agreement with the reference values reported in [60, 61] for bulk powder (i.e., standard BHVO-2). The significantly larger standard deviation of the micro-drilled BHVO-2G measurements, with respect to both micro-Sr SRM987 and BHVO-2 powder data, is likely partly related to small isotopic heterogeneities of the glass standard. The few available micro-Sr data on the same sample provide similar averages and reproducibility of our data [54, 62] (Table 3).

Comparing our results with LA-MC-ICPMS data is more difficult; in fact, the latter vary largely depending on the material used for the analyses. External reproducibility obtained with LA-MC-ICPMS on material with high Sr contents and low Rb/Sr (e.g., apatite [49, 53], marine shells, and synthetic plagioclase [16]) is comparable or slightly worse than that attained with our method; yet, small but significant differences in accuracy have been reported [53]. On the other hand, the internal and external reproducibility worsen significantly (e.g., by a factor 5 to 10 in [16]) in materials with low Sr and high Rb/Sr.

In summary, the method presented here generally provides more accurate and precise results than LA-MC-ICPMS, independently on the nature of the analysed material, despite being more time-consuming. It is therefore suitable for a wider range of applications.

3. Applications

In this section, we report three case studies, two of which were previously published [8, 10], as examples of possible applications of the presented methodology in different fields of science. Indeed, in the last decade, the in situ isotope microsampling approach has been used and applied in many pilot studies in a wide range of research fields, including, among others, palaeoenvironmental and palaeoecologic reconstructions (i.e., [53, 63]) and climate changes (i.e., [64]).

In the three presented case studies, the samples were thoroughly characterised both texturally (optical microscope and SEM) and chemically (electron micro probe analyses) before drilling. The strontium element concentrations (in ppm) in all the samples was then determined through LA-ICPMS.

3.1. Micro-Sr Isotope in Minerals. Rock-forming minerals in igneous rocks display variable chemical composition depending on several processes and parameters such as (i) the physicochemical conditions of the magmas, (ii) open system processes (e.g., magma mixing and mingling), and (iii) recycling of cumulated crystals triggered by new arrivals of magma within crustal reservoirs. Radiogenic isotope ratios in minerals, or portions of them, can be used as a petrogenetic "DNA" to record the history of the magma reservoir (*crystal isotope stratigraphy*, e.g., [7]) and their evolution within the crust (e.g., [1, 5, 7, 8, 65–67]). Combining in situ Sr-isotope fingerprints with other approaches, such as textural evidences and crystal size distribution, offers the opportunity to understand the processes and timescales through which magmas are stored, differentiated, and delivered prior to eruption (e.g., [5–7, 13, 14, 16, 18, 54, 68, 69]).

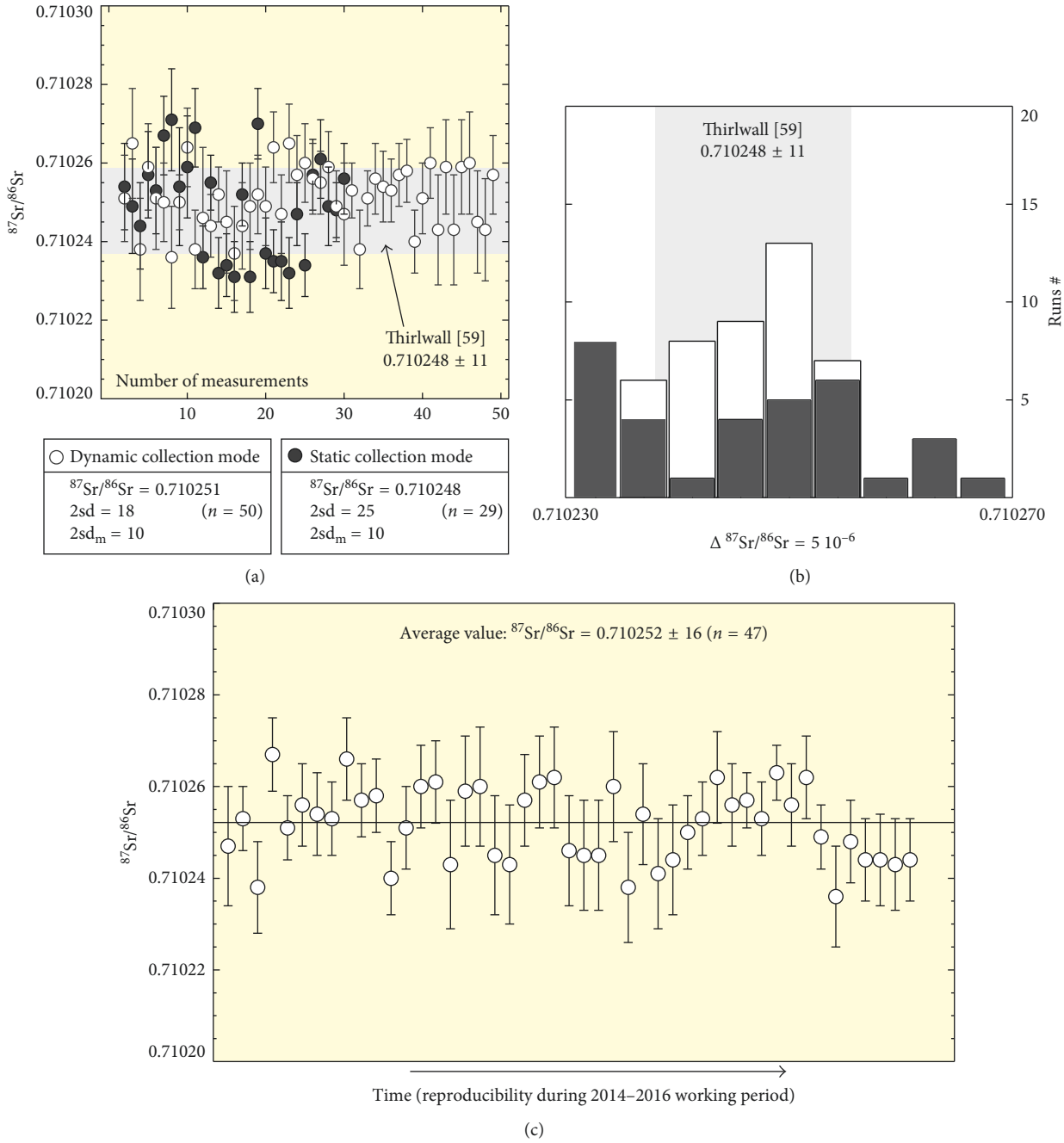

Figure 6: (a) Reproducibility and accuracy for repeated measurements of $^{87}Sr/^{86}Sr$ on 12 ng load size of NSIT-SRM987 standard material for static versus dynamic collection mode over a period of 10 months. Each single measurement is plotted with the relative error bars. The grey-shaded field shows the [59] recommended value range. (b) Distribution of the $^{87}Sr/^{86}Sr$ values measured all over the period of analysis with the static and dynamic collection mode: the static collection mode (black filled columns) shows a worst external reproducibility than that obtained in the dynamic mode (open columns); indeed the dynamic mode gives measurements that reasonably fit a Gaussian distribution pattern with the more representative $^{87}Sr/^{86}Sr$ values centered within the [59] recommended interval (grey shade fields); (c) reproducibility and accuracy trend of $^{87}Sr/^{86}Sr$ 12 ng load size of NSIT-SRM987 measured in the dynamic collection mode throughout the setup period (from 2014 to 2016).

The case study presented here is related to the active Nisyros volcano, the easternmost volcanic island of the South Aegean Active Volcanic Arc (Figure 7) [5, 70–76]. Nisyros volcanic products are typically porphyritic rocks, with clear petrographic evidence of recurrent mixing and mingling of different magmas during the whole volcano's history, which is likely interpreted as the triggering mechanism for its eruptions (e.g., [74, 77, 78]). Sr-isotope determinations at the subcrystal scale, along with detailed petrographic microscopic textural evidence, provided significant data for better defining the interaction of different magmas, concerning pre-eruptive mechanisms. The

Table 3: Accuracy and reproducibility on reference standard material (NIST-SRM987 and BHVO-2).

Standard	Sr content	$^{87}Sr/^{86}Sr$	2 SD	n	Reference
Within run measurement on international standard NIST-SRM987					
Large size loading (ng)					
SRM987	150	0.710253	0.000016	59	Long-term reproducibility (from 2013)
SRM987	150	0.710248	0.000011	427	Thirlwall [59]
Small size loading					
SRM987	10	0.710252	0.000016	47	This study
SRM987	12	0.710259	0.000018	92	Charlier et al. [54]
Drilling procedure on BHVO-2 glass					
BHVO-2 glass	<10	0.703490	0.000092	9	This study
BHVO-2 glass	10	0.703492	0.000094	3	Charlier et al. [54]
		$^{87}Sr/^{86}Sr$	2 SE		
BHVO-2 powder	150	0.703469	0.000004	1	This study
		$^{87}Sr/^{86}Sr$	2 SD		
BHVO-2 powder	—	0.703479	0.000020	12	Weis et al. [60]

2 SD, two standard deviation (external precision); 2 SE, two standard error of the mean; n, numbers of measurements; literature data are reported in italics below our mean values for references.

study focused, in particular, on postcaldera, rhyodacitic dome magmas of the final Nisyros activity emplaced after the caldera-forming rhyolitic explosive eruption of upper pumice. These rhyodacitic lavas contain magmatic enclaves (Figures 7(a) and 7(c)), with basaltic andesite to andesite compositions interpreted, based on their textural features, as quenched portions of mafic magmas included in the cooler, more evolved rhyodacitic host melt (Figures 7(b) and 7(c)) (e.g., [8, 78]).

In situ Sr-isotope ratios were determined on plagioclase phenocrysts (Figures 7(c)–7(e)), from both domes and enclaves, which preserve evidence of the complex history of interaction between the mafic (i.e., enclaves) and felsic (i.e., rhyodacitic domes) magmas in their growing zones [8]. The $^{87}Sr/^{86}Sr$ values determined on micromilled samples from the different growth zones of the plagioclase phenocrysts show clear Sr-isotope disequilibria between (i) cores and rims of single crystals (Figures 7(c)–7(e)) and (ii) the crystals and the host magmas (Figure 7(e)). This suggests that some of the phenocrysts that had formed in the rhyolitic magmas were later enclosed (as xenocrysts) within the more mafic one (i.e., as enclaves). Whereas the rim of the phenocrysts is isotopically intermediate between the rhyolitic and mafic magmas (Figure 7(f)), their cores show higher $^{87}Sr/^{86}Sr$ values, quite close to that of the previously erupted upper pumice magma. This clearly indicates that the phenocrysts originated in a different, older system. In this light, the large plagioclase phenocrysts found inside the dome lavas and enclaves can be interpreted as recycled from previously cumulated crystals (called "antecrysts" by Davidson et al. [7]).

These results have also demonstrated that the dome lavas are multicomponent magmas formed by progressive mingling/mixing processes between (i) a rhyolitic, and more Sr-radiogenic melt derived from the original upper pumice magmas, and (ii) the enclave-forming mafic, and less Sr-radiogenic, melts refilling the felsic magma chamber.

The constraints involved in interpreting in situ isotope data have further implications for the timing and style of eruption. The inferred delay between the mafic input (i.e., enclaves) and the relative dome eruption allows time for reheating and consequent drop in magma viscosity, thus favouring dome extrusion rather than explosive activity [8, 78].

3.2. Micro-Sr Isotope in Natural Glasses. Glasses are found in nature generated by rapid quenching of molten material. They represent a volumetrically small component of crustal rocks and can have different genesis (i.e., volcanic, lightning strikes, meteorite impact, and anthropogenic). In this light, the radiogenic isotopic compositions (i.e., Sr, Nd, and Pb) can provide fundamental information to discriminate among the processes involved in their formation. Glasses constitute the main component of ash and pyroclastic deposits, and their composition and Sr-isotope signature can provide important information in defining the triggering mechanisms of explosive eruptions (e.g., [10, 69, 79–84]). Glasses may also be found in ceramics, as well as in other artefacts. Sr-isotope data are therefore also important to define the possible source of raw materials for pottery, which is particularly relevant for cultural heritage, or to track trade routes in archaeology (e.g., [85–88]). Microscopic scale Sr-isotopic measurements on glasses would help in minimising the amount of sample that needs to be milled, which is of crucial importance both dealing with small-sized volcanic ashes and ejecta and with human artefact of archaeological interest.

The present study is a case study of submicroscopic scale Sr-isotopic determination on ashes of the 2010 Eyjafjallajökull (Iceland) volcano's explosive eruption, which caused enormous disruption to air travel across the northern hemisphere (Figure 8(a)) (e.g., [89–94]). This eruption represents a unique opportunity to test the potential of microscale Sr-isotope determinations on ash glasses from tephra deposits that were well preserved within the ice/snow pack [10]. The population of tephra is composed by four different types of ash fragments: (i) fluidal, (ii) coarsely vesicular, (iii) spongy fine vesicular, and (iv) blocky (Figure 8(b); [93]), generated by different fragmentation processes during the eruption. A detailed microanalytical geochemical and in situ Sr-isotope study performed on glassy groundmass of single ash clast showed unusually high $^{87}Sr/^{86}Sr$ values (up

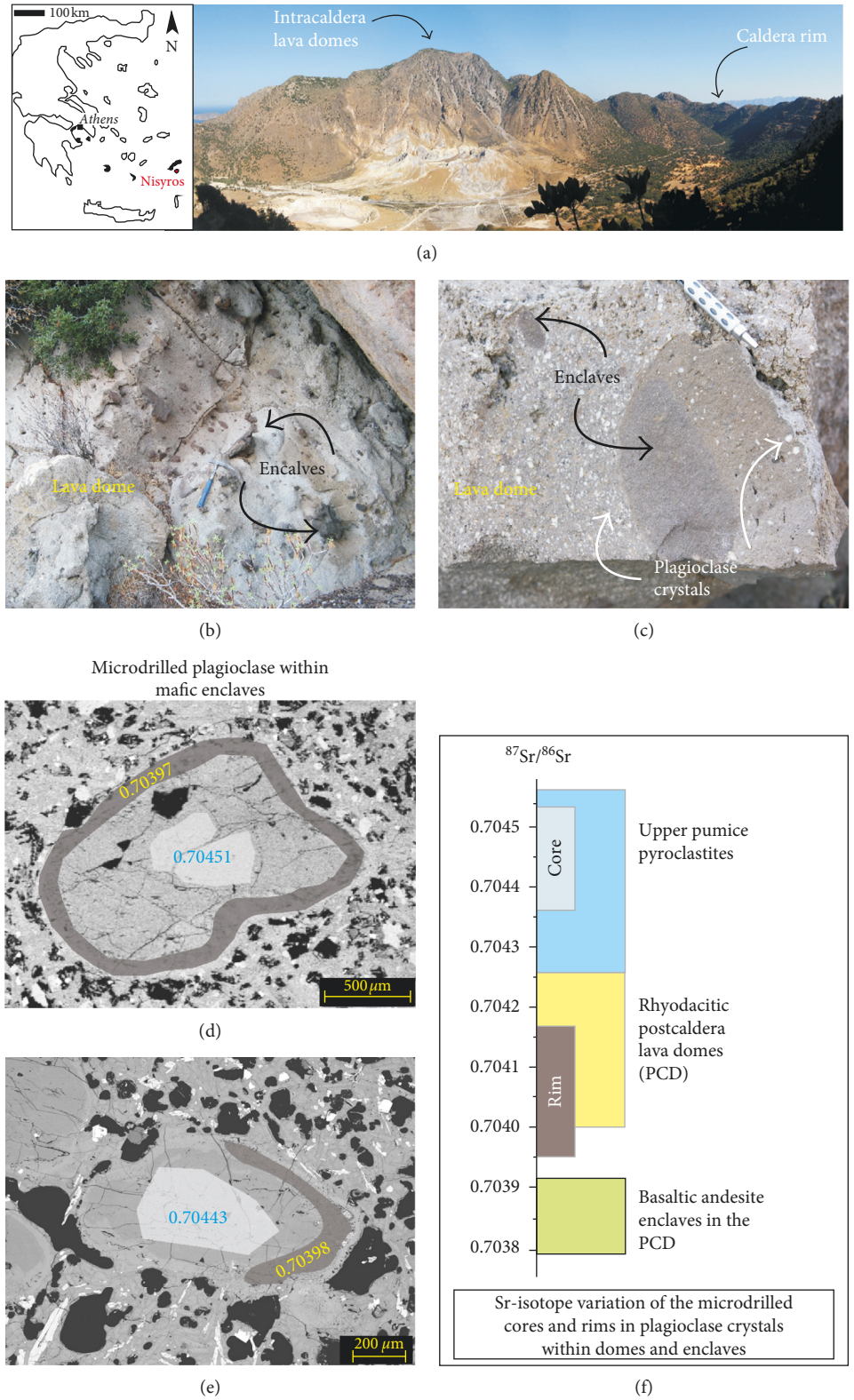

Figure 7: Results of micro-Sr isotope studies on plagioclase crystals from the last magmatic activity of Nisyros volcano (Greece). (a) Landscape view of the Nisyros caldera and its lava domes outpoured during the final magmatic activity of the volcano; (b) image of a lava dome outcrop rich in magmatic enclaves. Notably, the enclaves occurs as well-defined body with rounded and smooth surfaces; (c) specific image of a lava dome and enclave, both rich in large plagioclase crystals; (d and e) back-scattered electron microscope images of two representative plagioclase crystals selected for micro-Sr investigation with microdrill. The shaded areas represent the crystal zones drilled for Sr-isotope analyses, both on cores and rims; (f) $^{87}Sr/^{86}Sr$ variation of the drilled cores and rims compared to the range of $^{87}Sr/^{86}Sr$ of host whole rock (domes and enclaves) and upper pumice whole rock.

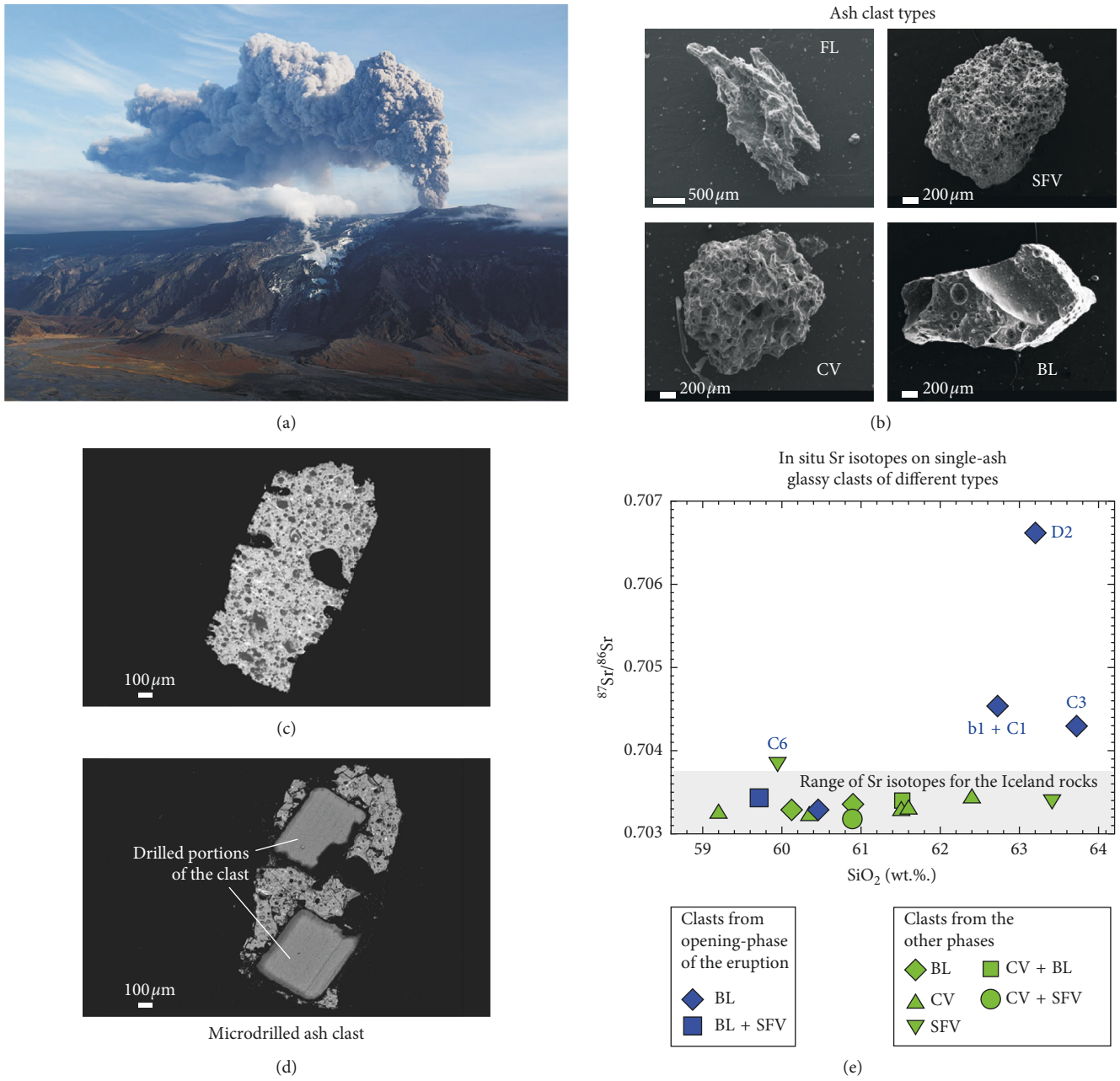

Figure 8: Results of micro-Sr isotopes in volcanic ash glasses of the 2010 explosive eruption of Eyjafjallajökull volcano (Iceland). (a) Spectacular image of the ash cloud erupted by the volcano during the early stage of the 2010 activity (https://hiticeland.com/places_and_photos_from_iceland/eyjafjallajokull causing); (b) back-scattered electron microscope images of different clast types sampled in the basal level of the fallout deposit related to the open phase of the 2010 eruption. FL = fluidal; SFV = spongy finely vesicular; CV = coarse vesicular; and BL = blocky. Scale bars are in micron; comparison between back-scattered electron microscope images of clasts before (c) and after (d) in situ microdrilling. Scale bars are in micron; (e) $^{87}Sr/^{86}Sr$ versus SiO_2 (wt.%) diagram of matrix glasses sampled from single, glassy ash clasts. In situ microsampling for Sr-isotope determinations on glass and plagioclase have been obtained by microdrilling technique. Error bars are inside the symbols.

to 0.70668) for Icelandic volcanism (0.7026–0.7037 [94]) (Figure 8(c)); these high isotopic values were also associated to atypical elemental compositions compared to most of the juvenile ash fragments of the eruption. The anomalous, high Sr-radiogenic clasts belong to the blocky type (Figure 8 (b)) and are concentrated in the first, thin ash level emplaced during the initial phase of eruptive activity. These clasts originated from the magma quenched from the contact with the ice cap filling the summit caldera of the volcano [10]. These anomalous findings in the Icelandic magmatic environment can be explained supposing that during its rise and before intruding into the ice cover, the erupting magma selectively assimilated hydrothermal minerals (i.e., zeolites, silica phases, and anhydrite) with seawater-

related high-Sr isotopic ratios, hosted in altered volcanic/epiclastic rocks. This selective assimilation took place at the tip edge of the first rising magma body, resulting in a high degree of contamination restricted to the rather small amount of melt directly in contact with the hydrothermal veins. Indeed, evidence for this process is recorded only by the very first erupted juveniles (i.e., the blocky clasts). The results obtained through submicroscopic-scale micromilling and relative Sr-isotope determination revealed the dynamics of the processes involved in the initial stages of magma ascent to the surface; this provides significant insights into the interpretation of the precursory signals of the eruption (mostly consisting of ground deformation or increased seismicity) [10]. These transient processes, which interested only a small, well-confined part of the magma, cannot be detected using traditional, Sr-isotope determination on whole-rock samples but can be revealed only analysing single-glassy clasts separately.

3.3. Micro-Sr Isotope in Teeth and Bones. Due to their similar chemical properties, Sr can substitute for Ca in the bioapatite [$Ca_5(PO_4,CO_3)_3(OH,F)$] of mammalian bones and teeth, reaching contents of few hundreds of ppm that allows the isotope analysis by microdrilling. The Sr isotope composition of human and animal hard tissues is a function of their dietary habits (e.g., [22]) and depends on the isotopic composition of the food and water ingested during life, which in turn are related to the geological substrate [95–97].

Sr isotopes have been successfully used, along with other stable and radiogenic isotope systematics (i.e., $\delta^{13}C$ and $\delta^{18}O$ and Pb isotopes), not only to track the source regions of migrants and migration pathways, as well as the hunting and trading areas of human populations, but also to study and define the dietary habits of humans and animals (e.g., [23, 44, 95–106]).

A pioneering study [107] demonstrated that migrant individuals who moved between different geologic regions might be traced by comparing $^{87}Sr/^{86}Sr$ in adult tooth enamel, formed between four and twelve years of age, and in the bones, which remodel throughout life and therefore representative of adulthood [30]. Unlike bones and dentine, dental enamel formed during childhood [108] remains unaltered throughout the years. Different $^{87}Sr/^{86}Sr$ in the teeth and bones of an individual may thus reflect the fact that it moved around the landscape passing through different isotopic environments during its youth and maturity [109, 110]. Teeth enamel is generally preferred to dentine and bones in the analysis of Sr concentrations and isotope ratios because it is virtually unaffected by postmortem diagenesis (e.g., [111–113]).

The micro-scale Sr-isotope measurements of samples obtained using the submicroscopic-scale micromill technique is perfectly able to discriminate between enamel and dentine in single-tooth samples. In addition, this technique increases the accuracy of sampling and also reduces the amount of specimen to be destroyed for high-precision Sr-isotope analysis.

Ursus spelaeus was an endemic, widespread European Late Pleistocene species. In contrast to many other taxa, it has fairly rich fossil records, especially thanks to its recurrent use of caves or shelters for winter hibernation [114–116]. Caves were frequently used by bears for many generations, and numerous individuals eventually died in them, so that significant quantities of their remains accumulated over considerable periods of time.

Many studies used stable isotopes to determine the dietary habits of living and extinct bears (e.g., [117–121]), but until now only a small number of papers have considered employing Sr isotopes to possibly elucidate the factors influencing habitat use and gain insights into the foraging behaviour of cave bears [122]. We report here the first $^{87}Sr/^{86}Sr$ data obtained through in situ microsampling on teeth and bones of *Ursus spelaeus* found in Grotta all'Onda cave. The study was aimed at defining the lifestyle and feeding behaviour of one of the most prominent European Late Pleistocene mammals [123–125].

Grotta all'Onda cave is located 708 m above sea level (a.s.l.) in the Apuan Alps nearby the village of Camaiore (Tuscany, Italy) (Figure 9), in a sub-Mediterranean habitat [126]. The cave opens at the base of the Tuscan Nappe, at the contact between the "Calcare a Rhaetavicula Contorta Formation" (i.e., Upper Triassic dolomitic-limestone of the Tuscan Nappe) and the "Argilliti Varicolori Formation" (i.e., Lower Cretaceous shales) (Figure 9). The Rhaetavicula Contorta Formation is a polygenic breccia, mainly including metamorphic clasts, known as "Brecce di Grotta all'Onda" (Figure 9) (http://www502.regione.toscana.it/geoscopio/geologia.html). The fossil remains of *Ursus spelaeus* were recovered during a 1999 excavation. Radiocarbon dating of bone yielded ages ranging from 38.22 to 38.28 ky (BP) [127]. Six different specimens were selected for Sr isotope analysis; these include three lower molars (SCT4, SCT5, and SCT6) from layers 7J4, 7J3, and 7J5, respectively and three metapodial bones, SCT 1 (third metacarpal), SCT 2 (fourth metatarsal), and SCT3 (fourth metatarsal), from layers 7J4, 7J5, and 7J3, respectively (Figures 9(c) and 10(a)–10(b)–10(c)–10(d)). Two whole soil (i.e., cave earth) samples, SCT7 and SCT8, were also collected from the representative layers 7J4 and 7J5 (Figure 9(c)).

All the three teeth had well-preserved dentin and very thin enamel layer (Figure 10). In contrast, the three bones were rather differently preserved and had different porosity. In particular, SCT3 was the most heavily mineralised and best preserved, whereas SCT1 was densely vacuolated and preserved higher amounts of organic components.

Major element analyses of these specimens revealed that the enamel bioapatite was more mineralised than that of dentin and bones. Moreover, the dentin bioapatite was found enriched in Sr and in other trace elements [128].

For the purpose of this study, dentin and enamel of the teeth and cortical sections of the bones from Grotta all'Onda were micromilled and analysed for micro-Sr isotope determination. The two soil samples were also processed for Sr-isotope determination using the traditional, large sample method [37, 55]. The $^{87}Sr/^{86}Sr$ data are reported in Table 4. Tooth enamel shows higher $^{87}Sr/^{86}Sr$ and lower Sr/Ca than

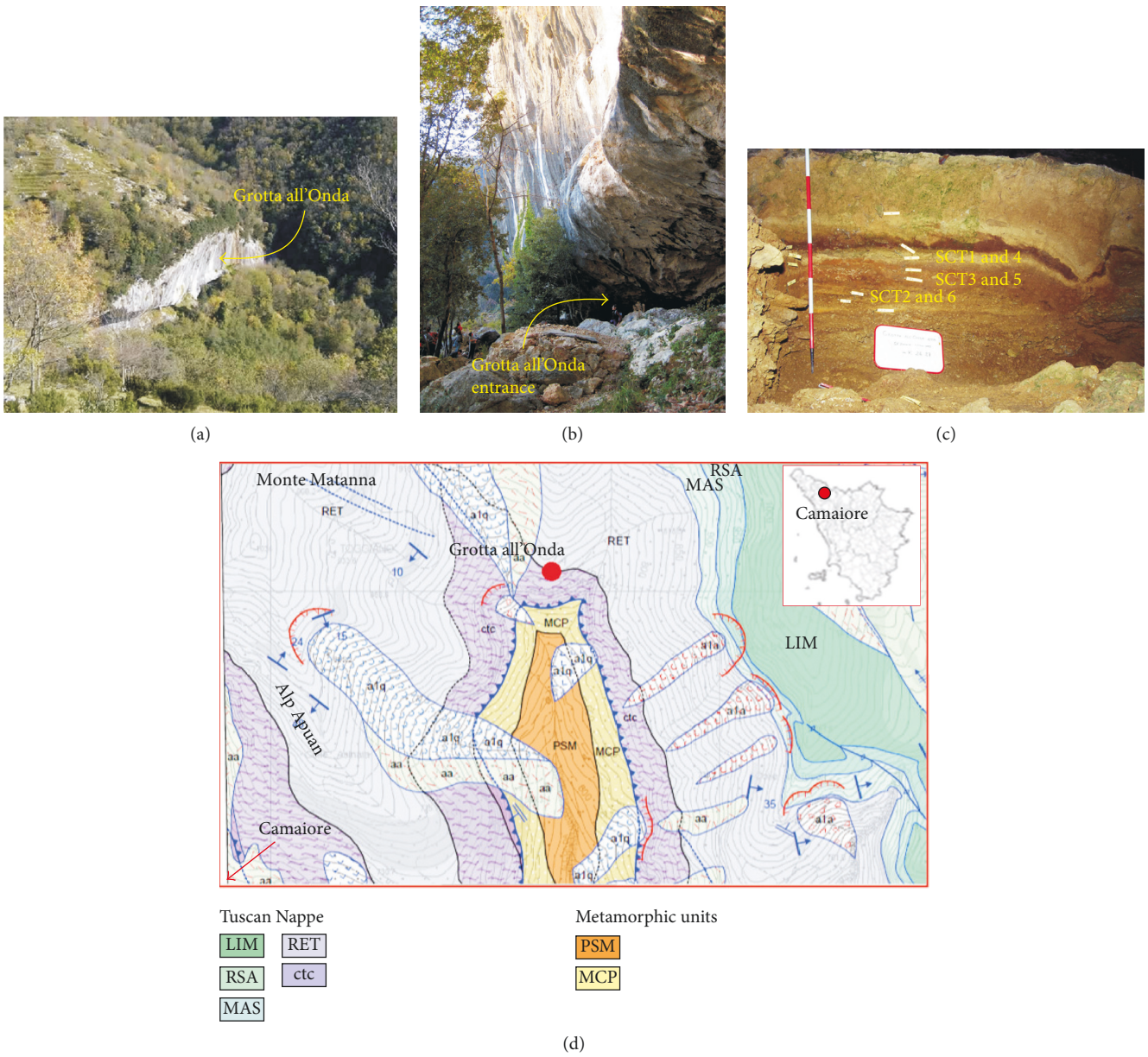

Figure 9: The *Ursus spelaeus* finding environment. (a) Image of the Grotta all'Onda cave from the above, showing the well-defined cut of the Mt. Matanna flank where the cave is located; (b) image of the entrance of the Grotta all'Onda cave; (c) image of the soil stratigraphy from which the *Ursus spelaeus* fossil remains have been sampled during the 1999 field campaign; (d) geological sketch map of the area around the Grotta all'Onda cave (http://www502.regione.toscana.it/geoscopio/geologia.html#). Formation of the Tuscan Nappe unit: LIM: "*Calcare Secifero di Limano*" formation; RSA: "*Rosso Ammonitico*" formation; MAS: "Calcare Massiccio" formation; RET: "*Raethavicola Contorta*" formation, Late Triassic dolomitic-limestones; ctc: cataclastic formation made by a polygenic breccias of mainly metamorphic limestone clasts. Tuscan metamorphic units: PSM: "Pseudomacigno" formation; MCP: "Cipollini" formation.

microsamples of dentin and bones do (Figures 10(e) and 10(f)). This strongly suggests that $^{87}Sr/^{86}Sr$ of tooth enamel is unaffected by diagenetic alteration, in contrast to the other organic-rich samples (i.e., bones and dentin). The $^{87}Sr/^{86}Sr$ composition of the dentin samples is close to that of the local soil samples (Figure 10(e)); even closer to the latter is that of the bone samples, with the only exception of SCT3 due to its high degree of mineralisation.

These results, despite the relatively recent age of the fossil specimens (ca. 40 ka [127]), indicate that bone tissues have been more exposed to *postmortem* diagenetic exchange processes compared to more heavily mineralized enamel. This speaks for a possible isotope reequilibration between dentin and bones (but not enamel) and soil, due to Sr exchange with percolating fluids. The soil samples have $^{87}Sr/^{86}Sr$ values comparable to those of the "Calcare a Rhaetavicula Contorta" formation, which forms the cave's bedrock [129], through which fluids filter into the cave (Figure 10(e)).

In summary, our study shows that the Grotta all'Onda bones and dentin are unsuitable to determine the

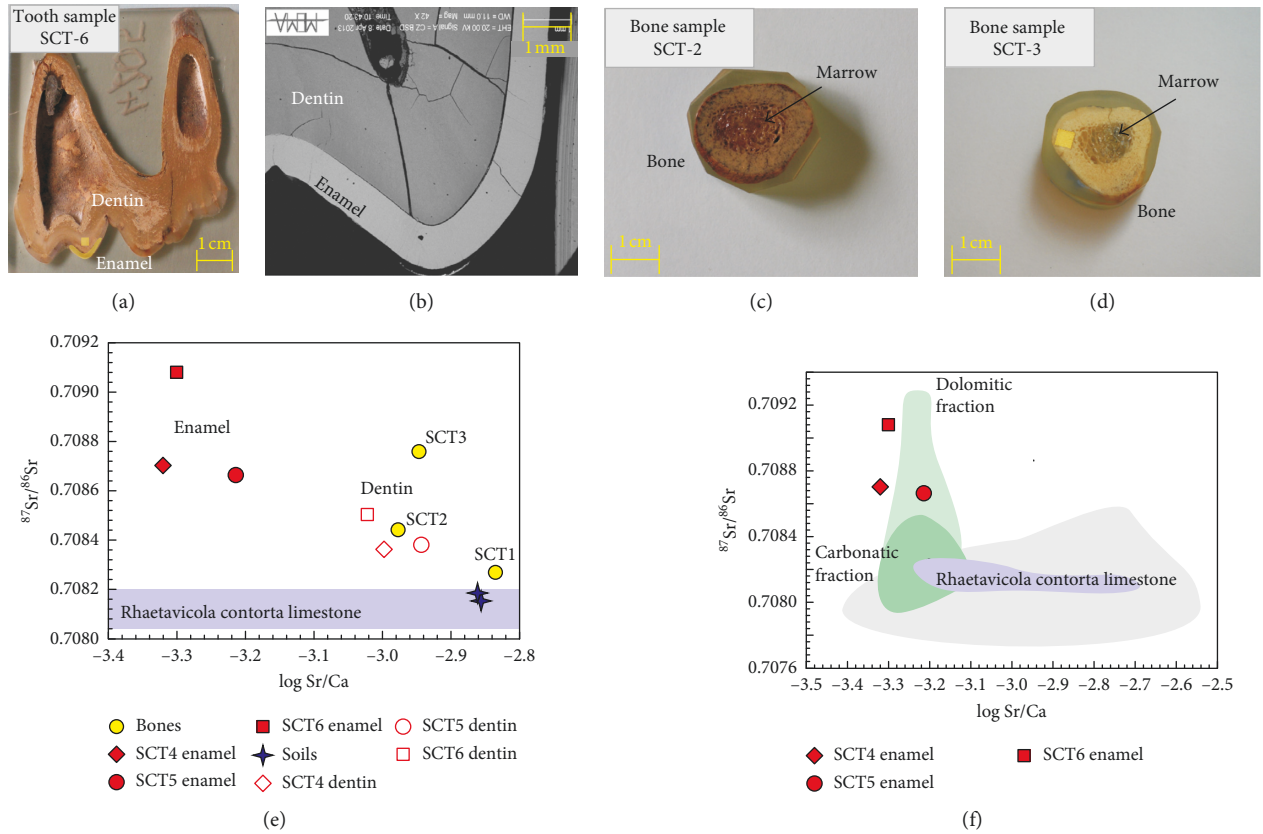

FIGURE 10: Results of micro-Sr isotopes in teeth and bones of the *Ursus spelaeus*. (a) Representative image of one tooth sample, sectioned for microdrilling. The thin layer of enamel is well evident with respect to the lighter inner dentin. In yellow are reported the two drilling sites on dentin and enamel; (b) particular back-scattered electron microscopy image of the edge of the tooth showing dentin (dark grey) and enamel (light grey) portion; (c and d) images of two of the analysed bones properly prepared in epoxy resin mounts for microdrilling sampling. In yellow is reported the drilling site; (e) $^{87}Sr/^{86}Sr$ versus Sr/Ca (in log scale) diagram showing the results obtained from the analyses of enamel and dentin in the three teeth, compared with bones of the *Ursus spelaeus* specimen. The $^{87}Sr/^{86}Sr$ of soils in which the fossils have been sampled are also reported together with the Sr-isotope field of the *Raetavicola Contorta* limestone for comparison. (See text for detail) (f) $^{87}Sr/^{86}Sr$ versus Sr/Ca (in log scale) diagram comparing the Sr-isotope values of dentin from the three teeth samples with the Sr-isotope range fields of the different geologic formations forming the bedrock outcropping in the area of the Grotta all'Onda cave.

TABLE 4: (a) $^{87}Sr/^{86}Sr$ results obtained on microsamples of tooth dentine and enamel and bones of the *Ursus spelaeus* specimen. (b) $^{87}Sr/^{86}Sr$ soils sampled in the Grotta all'Onda cave from which the fossil remains were collected.

Sample	Type	Sr content (ppm)	$^{87}Sr/^{86}Sr$	2 SE	Log (Sr/Ca) Average
(a) Teeth and bones					
STC1	Bone	510	0.708268	0.000006	−2.84
STC2	Bone	352	0.708441	0.000006	−2.98
STC3	Bone	359	0.708758	0.000006	−2.95
STC4-1	Enamel	187	0.708703	0.000005	−3.32
STC4-2	Dentin	360	0.708362	0.000006	−3.00
STC5-1	Enamel	211	0.708663	0.000005	−3.21
STC5-2	Dentin	384	0.708380	0.000006	−2.94
STC6-1	Enamel	179	0.709081	0.000005	−3.30
STC6-2	Dentin	339	0.708504	0.000006	−3.02
(b) Soils					
STC7	Soil	204	0.708184	0.000006	−2.86
STC8	Soil	228	0.708155	0.000006	−2.86

2 SE: two standard error of the mean.

characteristics of the habitat where the cave bear lived, due to their interaction with percolating water and their consequent contamination by the soils in which they had been preserved. In contrast, the $^{87}Sr/^{86}Sr$ ratios of the tooth enamel results unaltered and realistically reflects the original values achieved during the cave bear's life. The isotopic composition of the

enamel samples is consistent with that of the "Calcare Massiccio Formation" and in particular with the dolomite fraction [129] (Figure 10(f)). The mismatch between the $^{87}Sr/^{86}Sr$ values of the enamel samples and those of the cave soils (Figure 10(e)) (i.e., local substrata of the cave) indicate that the cave bear died away from its customary habitat. Bears cannot indeed find food in caves, where they find refuge as shelter for winter hibernation or for night resting. The enamel isotopic values obtained during our study indicate that *Ursus spelaeus* from Grotta all'Onda roamed in search for food within a confined area not far from the cave, where the "Calcare Massiccio" is largely exposed and did not move too far from the area during its whole life.

4. Summary and Conclusions

The present study show the potential of $^{87}Sr/^{86}Sr$ determination by TIMS on micro-scale samples, based on micromilling solid specimens, not only for geological applications, but also for other fields, such as archaeology, forensics, medical, and life sciences, where it has hardly, if ever, been used. Reported here is a detailed description of all the analytical protocols, including results on replicate analyses of international standards (SRM 987 and BHVO-2G), which yield good accuracy and precision. In addition, three case studies are presented, performed in our laboratory, where in situ microdrilled Sr isotopes have been used in different fields of application.

The first case study on micro-Sr isotope determination at subgrain microscopic scale regards the petrogenetic processes relevant to the understanding of the plumbing system dynamics under active volcanoes. This example revealed the role played by the interaction of different magmas, which are normally characterised by distinct $^{87}Sr/^{86}Sr$ signatures, comingled in the plumbing system of the Nisyros volcano, which was capable of triggering the eruption.

The second case regards volcanic glasses with extremely low total Sr content (i.e., tholeiitic). The micromilling determination of $^{87}Sr/^{86}Sr$ ratio was performed on ashes, with different shapes and nature, erupted by different phases, during the 2010 eruption of Eyjafjallajökull volcano (Iceland). The $^{87}Sr/^{86}Sr$ data provide information on the eruptive mechanism involved during the eruption, as well as on the interaction between the magma and the hydrothermally-derived minerals attained before the thawing of the ice cap; it also provides significant insights into the interpretation of the precursory signals of the eruption.

The third case displays the use of $^{87}Sr/^{86}Sr$ microdrilled in enamel, dentin, and bones, to show that only enamel has more chances to preserve the original Sr-isotope signatures than bone and dentin. The analysis also revealed the close relationship existing between the radiogenic-Sr of the organic materials and that of the geologic Cretaceous substratum of the Apuan Alps, which provides valuable insights into the palaeoenvironment of the local cave bears. In this case, the Sr isotopes proved particularly useful for determining the foraging habits of extinct mammals, which substantiates the well-known statement "YOU ARE WHAT YOU EAT" (cit. Anthelme Brillat-Savarin).

Conflicts of Interest

The authors declare that there are no conflicts of interest regarding the publication of this paper.

Authors' Contributions

Lorella Francalanci provided the input to the set-up and the development of the in situ micro-Sr isotope procedure at the Radiogenic Isotope Laboratory of Firenze, providing also continuous scientific stirring and encouraging to the other research fellows, coauthors of the present paper.

Acknowledgments

The research on volcanic rocks was financially supported by PRIN 2010-2011 and 2015 with Grants 2010TT22SC_001 and 20158A9CBM, respectively. Regione Toscana government supported the salary of Sara Di Salvo through a "Pegaso" fellowship. The studies on the *Ursus spelaeus* had no financial support, and the analytical work expenses were covered by the "Radiogenic Lab" of the University of Florence. The authors are grateful for the suggestions of an anonymous reviewer, which improved the paper.

References

[1] F. J. Tepley and J. P. Davidson, "Mineral-scale Sr-isotope constraints on magma evolution and chamber dynamics in the Rum layered intrusion, Scotland," *Contributions to Mineralogy and Petrology*, vol. 145, no. 5, pp. 628–641, 2003.

[2] G. Perini III, F. J. Tepley, J. P. Davidson, and S. Conticelli, "The origin of K-feldspar megacrysts hosted in alkaline potassic rocks from central Italy: a track for low-pressure processes in mafic magmas," *Lithos*, vol. 66, no. 3-4, pp. 223–240, 2003.

[3] D. Morgan, S. Blake, N. Rogers et al., "Time scales of crystal residence and magma chamber volume from modelling of diffusion profiles in phenocrysts: vesuvius 1944," *Earth and Planetary Science Letters*, vol. 222, no. 3-4, pp. 933–946, 2004.

[4] W. Siebel, E. Reitter, T. Wenzel, and U. Blaha, "Sr isotope systematics of K-feldspars in plutonic rocks revealed by the Rb-Sr microdrilling technique," *Chemical Geology*, vol. 222, no. 3-4, pp. 183–199, 2005.

[5] L. Francalanci, G. R. Davies, W. Lustenhouwer, S. Tommasini, P. R. Mason, and S. Conticelli, "Intra-grain Sr isotope evidence for crystal recycling and multiple magma reservoirs in the recent activity of Stromboli volcano, southern Italy," *Journal of Petrology*, vol. 46, no. 10, pp. 1997–2021, 2005.

[6] L. Francalanci, R. Avanzinelli, I. Nardini, M. Tiepolo, J. P. Davidson, and R. Vannucci, "Crystal recycling in the steady-state system of the active Stromboli volcano: a 2.5-ka story inferred from in situ Sr-isotope and trace element data," *Contributions to Mineralogy and Petrology*, vol. 163, no. 1, pp. 109–131, 2012.

[7] J. P. Davidson, D. J. Morgan, B. L. A. Charlier, R. Harlou, and J. M. Hora, "Microsampling and isotopic analysis of igneous rocks: implications for the study of magmatic systems," *Annual Review of Earth and Planetary Sciences*, vol. 35, no. 1, pp. 273–311, 2007.

[8] E. Braschi, L. Francalanci, S. Tommasini, and G. E. Vougioukalakis, "Unraveling the hidden origin and migration of plagioclase phenocrysts by in situ Sr isotopes: the case of final dome activity at Nisyros volcano, Greece," *Contributions to Mineralogy and Petrology*, vol. 167, no. 3, p. 988, 2014.

[9] S. Conticelli, E. Boari, L. Burlamacchi et al., "Geochemistry and Sr-Nd-Pb isotopes of Monte Amiata Volcano, Central Italy: evidence for magma mixing between high-K calc-alkaline and leucititic mantle-derived magmas," *Italian Journal of Geosciences*, vol. 134, no. 2, pp. 266–290, 2015.

[10] M. Pistolesi, R. Cioni, L. Francalanci et al., "The onset of an eruption: selective assimilation of hydrothermal minerals during pre-eruptive magma ascent of the 2010 summit eruption of Eyjafjallajökull volcano, Iceland," *Journal of Volcanology and Geothermal Research*, vol. 327, pp. 449–458, 2016.

[11] J. N. Christensen, A. N. Halliday, D. C. Lee, and C. M. Hall, "In situ Sr isotopic analysis by laser ablation," *Earth and Planetary Science Letters*, vol. 136, no. 1-2, pp. 79–85, 1995.

[12] J. P. Davidson and F. J. Tepley, "Recharge in volcanic systems: evidence from isotope profiles of phenocrysts," *Science*, vol. 275, no. 5301, pp. 826–829, 1997.

[13] J. P. Davidson, L. Font, B. L. Charlier, and F. J. Tepley, "Mineral-scale Sr isotope variation in plutonic rocks–a tool for unravelling the evolution of magma systems," *Earth and Environmental Science Transactions of the Royal Society of Edinburgh*, vol. 97, no. 4, pp. 357–367, 2006.

[14] B. L. A. Charlier, O. Bachmann, J. P. Davidson, M. A. Dungan, and D. J. Morgan, "The upper crustal evolution of a large silicic magma body: evidence from crystal-scale Rb–Sr isotopic heterogeneities in the Fish Canyon magmatic system, Colorado," *Journal of Petrology*, vol. 48, no. 10, pp. 1875–1894, 2007.

[15] B. L. Charlier, C. J. Wilson, and J. P. Davidson, "Rapid open-system assembly of a large silicic magma body: time-resolved evidence from cored plagioclase crystals in the Oruanui eruption deposits, New Zealand," *Contributions to Mineralogy and Petrology*, vol. 156, no. 6, pp. 799–813, 2008.

[16] J. P. Davidson, F. J. Tepley, Z. Palacz, and S. Meffan-Main, "Magma recharge, contamination, and residence times revealed by in situ laser ablation isotopic analysis of feldspar in volcanic rocks," *Earth and Planetary Science Letters*, vol. 184, no. 2, pp. 427–442, 2001.

[17] F. J. Tepley, J. P. Davidson, R. I. Tilling, and J. G. Arth, "Magma mixing, recharge and eruption histories recorded in plagioclase phenocrysts from El Chichon Volcano, Mexico," *Journal of Petrology*, vol. 41, no. 9, pp. 1397–1411, 2000.

[18] D. J. Morgan, D. A. Jerram, D. G. Chertkoff et al., "Combining CSD and isotopic microanalysis: magma supply and mixing processes at Stromboli Volcano, Aeolian Islands, Italy," *Earth and Planetary Science Letters*, vol. 260, no. 3-4, pp. 419–431, 2007.

[19] P. Horn, P. Schaaf, B. Holbach, S. Hölzl, and H. Eschnauer, "$^{87}Sr/^{86}Sr$ from rock and soil into vine and wine," *Zeitschrift für Lebensmitteluntersuchung und-Forschung A*, vol. 196, no. 5, pp. 407–409, 1993.

[20] J. L. Banner and J. Kaufman, "The isotopic record of ocean chemistry and diagenesis preserved in non-luminescent brachiopods from Mississippian carbonate rocks, Illinois and Missouri," *Geological Society of America Bulletin*, vol. 106, no. 8, pp. 1074–1082, 1994.

[21] G. Åberg, G. Fosse, and H. Stray, "Man, nutrition and mobility: a comparison of teeth and bone from the Medieval era and the present from Pb and Sr isotopes," *Science of the Total Environment*, vol. 224, no. 1, pp. 109–119, 1998.

[22] R. C. Capo, B. W. Stewart, and O. A. Chadwick, "Strontium isotopes as tracers of ecosystem processes: theory and methods," *Geoderma*, vol. 82, no. 1–3, pp. 197–225, 1998.

[23] B. L. Beard and C. M. Johnson, "Strontium isotope composition of skeletal material can determine the birth place and geographic mobility of humans and animals," *Journal of Forensic Science*, vol. 45, no. 5, pp. 1049–1061, 2000.

[24] S. Tommasini, G. R. Davies, and T. Elliott, "Lead isotope composition of tree rings as bio-geochemical tracers of heavy metal pollution: a reconnaissance study from Firenze, Italy," *Applied Geochemistry*, vol. 15, no. 7, pp. 891–900, 2000.

[25] M. Vanhaeren, F. d'Errico, I. Billy, and F. Grousset, "Tracing the source of Upper Palaeolithic shell beads by strontium isotope dating," *Journal of Archaeological Science*, vol. 31, no. 10, pp. 1481–1488, 2004.

[26] C. M. R. Almeida and M. T. S. Vasconcelos, "Lead contamination in Portuguese red wines from the Douro region: from the vineyard to the final product," *Journal of Agricultural and Food Chemistry*, vol. 51, no. 10, pp. 3012–3023, 2003.

[27] J. A. Evans and S. Tatham, "Defining "local signature" in terms of Sr isotope composition using a tenth-to twelfth-century Anglo-Saxon population living on a Jurassic clay-carbonate terrain, Rutland, UK," *Geological Society, London, Special Publications*, vol. 232, no. 1, pp. 237–248, 2004.

[28] S. Hölzl, P. Horn, A. Rossmann, and S. Rummel, "Isotope-abundance ratios of light (bio) and heavy (geo) elements in biogenic tissues: methods and applications," *Analytical and Bioanalytical Chemistry*, vol. 378, no. 2, pp. 270–272, 2004.

[29] S. Kelly, K. Heaton, and J. Hoogewerff, "Tracing the geographical origin of food: the application of multi-element and multi-isotope analysis," *Trends in Food Science & Technology*, vol. 16, no. 12, pp. 555–567, 2005.

[30] R. A. Bentley and C. Knipper, "Geographical patterns in biologically available strontium, carbon and oxygen isotope signatures in prehistoric SW Germany," *Archaeometry*, vol. 47, no. 3, pp. 629–644, 2005.

[31] P. Degryse, J. Schneider, U. Haack et al., "Evidence for glass "recycling" using Pb and Sr isotopic ratios and Sr-mixing lines: the case of early Byzantine Sagalassos," *Journal of Archaeological Science*, vol. 33, no. 4, pp. 494–501, 2006.

[32] S. Rummel, S. Hoelzl, P. Horn, A. Rossmann, and C. Schlicht, "The combination of stable isotope abundance ratios of H, C, N and S with $^{87}Sr/^{86}Sr$ for geographical origin assignment of orange juices," *Food Chemistry*, vol. 118, no. 4, pp. 890–900, 2010.

[33] S. Vorkelius, G. D. Lorenz, S. Rummel et al., "Strontium isotopic signatures of natural mineral waters, the reference to a simple geological map and its potential for authentication of food," *Food Chemistry*, vol. 118, no. 4, pp. 933–940, 2010.

[34] B. P. Kennedy, A. Klaue, J. D. Blum, C. L. Folt, and K. H. Nislow, "Reconstructing the lives of fish using Sr isotopes in otoliths," *Canadian Journal of Fisheries and Aquatic Sciences*, vol. 59, no. 6, pp. 925–929, 2011.

[35] C. Durante, C. Baschieri, L. Bertacchini et al., "Geographical traceability based on $^{87}Sr/^{86}Sr$ indicator: a first approach for PDO Lambrusco wines from Modena," *Food Chemistry*, vol. 141, no. 3, pp. 2779–2787, 2013.

[36] S. Marchionni, E. Braschi, S. Tommasini et al., "High-precision $^{87}Sr/^{86}Sr$ analyses in wines and their use as a geological fingerprint for tracing geographic provenance," *Journal of*

Agricultural and Food Chemistry, vol. 61, no. 28, pp. 6822–6831, 2013.

[37] S. Marchionni, A. Buccianti, A. Bollati et al., "Conservation of $^{87}Sr/^{86}Sr$ isotopic ratios during the winemaking processes of "Red" wines to validate their use as geographic tracer," *Food Chemistry*, vol. 190, pp. 777–785, 2016.

[38] V. Vinciguerra, R. Stevenson, K. Pedneault, A. Poirier, J.-F. Hélie, and D. Widory, "Strontium isotope characterization of wines from Quebec, Canada," *Food Chemistry*, vol. 210, pp. 121–128, 2016.

[39] P. L. Koch, J. Heisinger, C. Moss, R. W. Carlson, M. L. Fogel, and A. K. Behrensmeyer, "Isotopic tracking of change in diet and habitat use in African elephants," *Science*, vol. 267, no. 5202, p. 1340, 1995.

[40] A. Sillen, G. Hall, and R. Armstrong, "Strontium calcium ratios (Sr/Ca) and strontium isotopic ratios ($^{87}Sr/^{86}Sr$) of *Australopithecus robustus* and *Homo* sp. From Swartkrans," *Journal of Human Evolution*, vol. 28, no. 3, pp. 277–285, 1995.

[41] G. Grupe, "Preservation of collagen in bone from dry, Sandy soil," *Journal of Archaeological Science*, vol. 22, no. 2, pp. 193–199, 1995.

[42] G. Grupe, T. D. Price, and F. Söllner, "Mobility of Bell Beaker people revealed by strontium isotope ratios of tooth and bone: a study of southern Bavarian skeletal remains. A reply to the comment by Peter Horn and Dieter Müller-Sohnius," *Applied Geochemistry*, vol. 14, no. 2, pp. 271–275, 1999.

[43] P. Willey, A. Galloway, and L. Snyder, "Bone mineral density and survival of elements and element portions in the bones of the Crow Creek massacre victims," *American Journal of Physical Anthropology*, vol. 104, no. 4, pp. 513–528, 1997.

[44] K. A. Hoppe, P. L. Koch, R. W. Carlson, and S. D. Webb, "Tracking mammoths and mastodons: reconstruction of migratory behavior using strontium isotope ratios," *Geology*, vol. 27, no. 5, pp. 439–442, 1999.

[45] T. D. Price, J. H. Burton, and R. A. Bentley, "The characterization of biologically available strontium isotope ratios for the study of prehistoric migration," *Archaeometry*, vol. 44, no. 1, pp. 117–135, 2002.

[46] R. A. Bentley, T. D. Price, and E. Stephan, "Determining the "local" $^{87}Sr/^{86}Sr$ range for archaeological skeletons: a case study from Neolithic Europe," *Journal of Archaeological Science*, vol. 31, no. 4, pp. 365–375, 2004.

[47] J. A. Evans, J. Montgomery, G. Wildman, and N. Boulton, "Spatial variations in biosphere $^{87}Sr/^{86}Sr$ in Britain," *Journal of the Geological Society*, vol. 167, no. 1, pp. 1–4, 2010.

[48] J. H. Burton and T. D. Price, "Seeking the local $^{87}Sr/^{86}Sr$ ratio to determine geographic origins of humans," in *ACS Symposium Series*, pp. 309–320, ACS Publication, Washington, DC, USA, 2013.

[49] F. Lugli, A. Cipriani, C. Peretto, M. Mazzucchelli, and D. Brunelli, "In situ high spatial resolution $^{87}Sr/^{86}Sr$ ratio determination of two Middle Pleistocene (ca 580 ka) *Stephanorhinus hundsheimensis* teeth by LA–MC–ICP–MS," *International Journal of Mass Spectrometry*, vol. 412, pp. 38–48, 2017.

[50] T. Prohaska, C. Latkoczy, G. Schultheis, M. Teschler-Nicola, and G. Stingeder, "Investigation of Sr isotope ratios in prehistoric human bones and teeth using laser ablation ICP-MS and ICP-MS after Rb/Sr separation," *Journal of Analytical Atomic Spectrometry*, vol. 17, no. 8, pp. 887–891, 2002.

[51] S. R. Copeland, M. Sponheimer, P. J. le Roux et al., "Strontium isotope ratios ($^{87}Sr/^{86}Sr$) of tooth enamel: a comparison of solution and laser ablation multicollector inductively coupled plasma mass spectrometry methods," *Rapid Communications in Mass Spectrometry*, vol. 22, no. 20, pp. 3187–3194, 2008.

[52] A. Simonetti, M. R. Buzon, and R. A. Creaser, "In situ elemental and Sr isotope investigation of human tooth enamel by Laser Ablation-(MC)-ICP-MS: success and pitfalls," *Archaeometry*, vol. 50, no. 2, pp. 371–385, 2008.

[53] J. Lewis, C. D. Coath, and A. W. G. Pike, "An improved protocol for $^{87}Sr/^{86}Sr$ by laser ablation multi-collector inductively coupled plasma mass spectrometry using oxide reduction and a customised plasma interface," *Chemical Geology*, vol. 390, pp. 173–181, 2014.

[54] B. L. A. Charlier, C. Gimbre, D. Morgan et al., "Methods of microsampling and high-precision analysis of strontium and rubidium isotopes at single crystal scale for petrological and geochronological applications," *Chemical Geology*, vol. 232, no. 3-4, pp. 144–133, 2006.

[55] R. Avanzinelli, E. Boari, S. Conticelli et al., "High precision Sr, Nd, and Pb isotopic analyses using the new generation Thermal Ionisation Mass Spectrometer ThermoFinningan Triton-Ti®," *Periodico di Mineralogia*, vol. 74, no. 3, pp. 147–166, 2005.

[56] D. L. Hoffmann, C. Spötl, and A. Mangini, "Micromill and in situ laser ablation sampling techniques for high spatial resolution MC-ICPMS U-Th dating of carbonates," *Chemical Geology*, vol. 259, no. 3-4, pp. 253–261, 2009.

[57] A. Eberhart, R. Delwiche, and Z. Geiss, "Isotopic effects in single filament thermal ion sources," *Zeitschrift für Naturforschung A*, vol. 19, no. 6, pp. 736–740, 1964.

[58] W. A. Russel, D. A. Papanastassiou, and T. A. Tombrello, "Ca isotope fractionation on the Earth and other solar system materials," *Geochimica et Cosmochimica Acta*, vol. 42, no. 8, pp. 1075–1090, 1978.

[59] M. F. Thirlwall, "Long-term reproducibility of multicollector Sr and Nd isotope ratio analysis," *Chemical Geology*, vol. 94, no. 2, pp. 85–104, 1991.

[60] D. Weis, B. Kieffer, C. Maerschalk et al., "High-precision isotopic characterization of USGS reference materials by TIMS and MC-ICP-MS," *Geochemistry, Geophysics, Geosystems*, vol. 7, no. 8, 2006.

[61] J. B. Mahoney, D. Weiss, B. Keiffer et al., "Ongoing isotopic characterization of USGS standards: MC-ICPMS and TIMS data from the Pacific Centre for isotopic and geochemical research, University of British Columbia," in *Proceedings of Geological Society of America, Seattle Annual Meeting, Paper 117-118*, Seattle, WA, USA, October 2003.

[62] M. Elburg, P. Vroon, B. van der Wagt, and A. Tchalikian, "Sr and Pb isotopic composition of five USGS glasses (BHVO-2G, BIR-1G, BCR-2G, TB-1G, NKT-1G)," *Chemical Geology*, vol. 223, no. 4, pp. 196–207, 2005.

[63] C. Spötl and D. Mattey, "Stable isotope microsampling of speleothems for palaeoenvironmental studies: a comparison of microdrill, micromill and laser ablation techniques," *Chemical Geology*, vol. 235, no. 1-2, pp. 48–58, 2006.

[64] C. Saenger, R. I. Gabitov, J. Farmer, J. M. Watkins, and R. Stone, "Linear correlations in bamboo coral $\delta^{13}C$ and $\delta^{18}O$ sampled by SIMS and micromill: evaluating paleoceanographic potential and biomineralization mechanisms using δ^{11} B and Δ_{47} composition," *Chemical Geology*, vol. 454, pp. 1–14, 2017.

[65] K. M. Knesel, J. P. Davidson, and W. A. Duffield, "Evolution of silicic magma through assimilation and subsequent recharge: evidence from Sr isotopes in sanidine phenocrysts, Taylor Creek Rhyolite, NM," *Journal of Petrology*, vol. 40, no. 5, pp. 773–786, 1999.

[66] G. S. Wallace and G. W. Bergantz, "Reconciling heterogeneity in crystal zoning data: an application of shared characteristic diagrams at Chaos Crags, Lassen Volcanic Center, California," *Contributions to Mineralogy and Petrology*, vol. 149, no. 1, pp. 98–112, 2005.

[67] O. Bachmann and G. W. Bergantz, "Gas percolation in upper-crustal silicic crystal mushes as a mechanism for upward heat advection and rejuvenation of near-solidus magma bodies," *Journal of Volcanology and Geothermal Research*, vol. 149, no. 1-2, pp. 85–102, 2006.

[68] L. Font, J. P. Davidson, D. G. Pearson, G. M. Nowell, D. A. Jerram, and C. J. Ottley, "Sr and Pb isotope micro-analysis of plagioclase crystals from Skye lavas: an insight into open-system processes in a flood basalt province," *Journal of Petrology*, vol. 49, no. 8, pp. 1449–1471, 2008.

[69] V. M. Martin, J. Davidson, D. Morgan, and D. A. Jerram, "Using the Sr isotope compositions of feldspars and glass to distinguish magma system components and dynamics," *Geology*, vol. 38, no. 6, pp. 539–542, 2010.

[70] G. M. Di Paola, "Volcanology and petrology of Nisyros island (Dodecanese Greece)," *Bulletin Volcanologique*, vol. 38, no. 3, pp. 944–987, 1974.

[71] G. P. Wyers and M. Barton, "Polybaric evolution of calc-alkaline magmas from Nisyros, southeastern Hellenic Arc, Greece," *Journal of Petrology*, vol. 30, no. 1, pp. 1–37, 1989.

[72] K. S. Seymour and D. Vlassopoulos, "Magma mixing at Nisyros volcano, as inferred from incompatible trace-element systematics," *Journal of Volcanology and Geothermal Research*, vol. 50, no. 3, pp. 273–299, 1992.

[73] G. Vougioukalakis, "Volcanic stratigraphy and evolution of Nisyros island," *Bulletin of the Geological Society of Greece*, vol. 28, no. 2, pp. 239–258, 1993.

[74] L. Francalanci, J. C. Varekamp, E. G. Vougioukalakis, M. J. Defant, F. Innocenti, and P. Manetti, "Crystal retention, fractionation and crustal assimilation in a convecting magma chamber, Nisyros Voclano, Greece," *Bulletin of Volcanology*, vol. 56, no. 8, pp. 601–620, 1995.

[75] L. Francalanci, J. C. Varekamp, E. G. Vougioukalakis, F. Innocenti, and P. Manetti, "Is there a compositional gap at Nisyros volcano? A comment on: magma generation at the easternmost section of the Hellenic arc: Hf, Nd, Pb and Sr isotope geochemistry of Nisyros and Yali volcanoes (Greece)," *Lithos*, vol. 95, no. 3-4, pp. 458–461, 2007.

[76] C. Longchamp, A. Skopelitis, C. Bonadonna, and O. Bachmann, "Characterization of tephra deposits with limited exposure: the example of the two largest explosive eruptions at Nisyros volcano (Greece)," *Bulletin of Volcanology*, vol. 73, no. 9, pp. 1337–1352, 2011.

[77] E. M. Limburg and J. C. Varekamp, "Young pumice deposits on Nisyros, Greece," *Bulletin of Volcanology*, vol. 54, no. 1, pp. 68–77, 1991.

[78] E. Braschi, L. Francalanci, and G. E. Vougioukalakis, "Inverse differentiation pathway by multiple mafic magma refilling in the last magmatic activity of Nisyros Volcano, Greece," *Bulletin of Volcanology*, vol. 74, no. 5, pp. 1083–1100, 2012.

[79] M. Rautenschlein, G. A. Jenner, J. Hertogen et al., "Isotopic and trace element composition of volcanic glasses from the Akaki Canyon, Cyprus: implications for the origin of the Troodos ophiolite," *Earth and Planetary Science Letters*, vol. 75, no. 4, pp. 369–383, 1985.

[80] N. Blum and J. H. Crocket, "Repetitive cyclical volcanism in the Late Archean Larder Lake Group near Kirkland Lake, Ontario: implications of geochemistry on magma genesis," *Precambrian Research*, vol. 54, no. 2-4, pp. 173–194, 1992.

[81] M. F. Roden, T. Trull, S. R. Hart, and F. A. Frey, "New He, Nd, Pb, and Sr isotopic constraints on the constitution of the Hawaiian plume: results from Koolau Volcano, Oahu, Hawaii, USA," *Geochimica et Cosmochimica Acta*, vol. 58, no. 5, pp. 1431–1440, 1994.

[82] P. R. Castillo, E. Klein, J. Bender et al., "Petrology and Sr, Nd, and Pb isotope geochemistry of mid-ocean ridge basalt glasses from the 11 45′ N to 15 00′ N segment of the East Pacific Rise," *Geochemistry, Geophysics, Geosystems*, vol. 1, no. 11, 2000.

[83] L. Melluso, V. Morra, P. Brotzu et al., "Geochronology and petrogenesis of the Cretaceous Antampombato–Ambatovy complex and associated dyke swarm, Madagascar," *Journal of Petrology*, vol. 46, no. 10, pp. 1963–1996, 2005.

[84] G. Conde, P. D. Ihinger, and E. E. Frahm, "Water speciation in Anatolian Obsidian: quenched magmatic water vs low temperature hydration," *Geochimica et Cosmochimica Acta*, vol. 73, p. A239, 2009.

[85] P. Degryse, A. Boyce, N. E. Satullo et al., "Isotopic discriminants between late Bronze Age glasses from Egypt and the Near East," *Archaeometry*, vol. 52, no. 3, pp. 380–388, 2010.

[86] J. Henderson, J. Evans, and K. Nikita, "Isotopic evidence for the primary production, provenance and trade of Late Bronze Age glass in the Mediterranean," *Mediterranean Archaeology and Archaeometry*, vol. 10, no. 1, pp. 1–24, 2010.

[87] M. Ganio, K. Latruwe, D. Brems, P. Muchez, F. Vanhaecke, and P. Degryse, "The Sr–Nd isolation procedure for subsequent isotopic analysis using multi-collector ICP-mass spectrometry in the context of provenance studies on archaeological glass," *Journal of Analytical Atomic Spectrometry*, vol. 27, no. 8, pp. 1335–1341, 2012.

[88] E. Gliozzo, E. Braschi, F. Giannetti, A. Langone, and M. Turchiano, "New geochemical and isotopic insights into the Late Antique Apulian glass and the HIMT1 and HIMT2 glass productions—the glass vessels from San Giusto (Foggia, Italy) and the diagrams for provenance studies," *Archaeological and Anthropological Sciences*, pp. 1–30, 2017.

[89] F. Sigmundsson, S. Hreinsdóttir, A. Hooper et al., "Intrusion triggering of the 2010 Eyjafjallajokull explosive eruption," *Nature*, vol. 468, no. 7322, pp. 426–430, 2010.

[90] E. Kaminski, S. Tait, F. Ferrucci, M. Martet, B. Hirn, and P. Husson, "Estimation of ash injection in the atmosphere by basaltic volcanic plumes: the case of the Eyjafjallajökull 2010 eruption," *Journal of Geophysical Research: Solid Earth*, vol. 116, no. 9, 2011.

[91] M. T. Gudmundsson, T. Thordarson, A. Höskuldsson et al., "Ash generation and distribution from the April-May 2010 eruption of Eyjafjallajökull, Iceland," *Scientific Reports*, vol. 2, no. 1, p. 572, 2012.

[92] P. W. Webley, T. Steensen, M. Stuefer, G. Grell, S. Freita, and M. Pavolonis, "Analyzing the Eyjafjallajökull 2010 eruption using satellite remote sensing, lidar and WRF-Chem dispersion and tracking model," *Journal of Geophysical Research: Atmospheres*, vol. 117, no. 20, 2012.

[93] R. Cioni, M. Pistolesi, A. Bertagnini, C. Bonadonna, A. Hoskuldsson, and B. Scateni, "Insights into the dynamics and evolution of the 2010 Eyjafjallajökull summit eruption (Iceland) provided by volcanic ash textures," *Earth and Planetary Science Letters*, vol. 394, pp. 111–123, 2014.

[94] O. Sigmarsson, J. Maclennan, and M. Carpentier, "Geochemistry of igneous rocks in Iceland: a review," *Jökull*, vol. 58, pp. 139–160, 2008.

[95] T. D. Price, S. Nakamura, S. Suzuki, J. H. Burton, and V. Tiesler, "New isotope data on Maya mobility and enclaves at Classic Copan, Honduras," *Journal of Anthropological Archaeology*, vol. 36, pp. 32–47, 2014.

[96] P. A. Slater, K. M. Hedman, and T. E. Emerson, "Immigrants at the Mississippian polity of Cahokia: strontium isotope evidence for population movement," *Journal of Archaeological Science*, vol. 44, pp. 117–127, 2014.

[97] A. J. Waterman, D. W. Peate, A. M. Silva, and J. T. Thomas, "In search of homelands: using strontium isotopes to identify biological markers of mobility in late prehistoric Portugal," *Journal of Archaeological Science*, vol. 42, pp. 119–127, 2014.

[98] A. L. Rheingold, S. Hues, and M. N. Cohen, "Strontium and zinc content in bone as an indication of diet," *Journal of Chemical Education*, vol. 60, no. 3, pp. 233-234, 1983.

[99] C. Gilbert, J. Sealy, and A. Sillen, "An investigation of barium, calcium and strontium as palaeodietary indicators in the Southwestern Cape, South Africa," *Journal of Archaeological Science*, vol. 21, no. 2, pp. 173–184, 1994.

[100] T. D. Price, C. M. Johnson, J. A. Ezzo, J. Ericson, and J. H. Burton, "Residential mobility in the prehistoric southwest United States: a preliminary study using strontium isotope analysis," *Journal of Archaeological Science*, vol. 21, no. 3, pp. 315–330, 1994.

[101] T. D. Price, L. Manzanilla, and W. D. Middleton, "Immigration and the ancient city of Teotihuacan in Mexico: a study using strontium isotope ratios in human bone and teeth," *Journal of Archaeological Science*, vol. 27, no. 10, pp. 903–913, 2000.

[102] J. H. Burton, T. D. Price, L. Cahue, and L. E. Wright, "The use of barium and strontium abundances in human skeletal tissues to determine their geographic origin," *International Journal of Osteoarchaeology*, vol. 13, no. 1-2, pp. 88–95, 2003.

[103] D. Mueller and E. Heinzle, "Stable isotope-assisted metabolomics to detect metabolic flux changes in mammalian cell cultures," *Current Opinion in Biotechnology*, vol. 24, no. 1, pp. 54–59, 2013.

[104] T. Tütken and T. Vennemann, "Stable isotope ecology of Miocene large mammals from Sandelzhausen, southern Germany," *Paläontologische Zeitschrift*, vol. 83, no. 1, pp. 207–226, 2009.

[105] L. A. Gregoricka, "Residential mobility and social identity in the periphery: strontium isotope analysis of archaeological tooth enamel from southeastern Arabia," *Journal of Archaeological Science*, vol. 40, no. 1, pp. 452–464, 2013.

[106] E. McManus, J. Montgomery, J. Evans, A. Lamb, R. Brettell, and J. Jelsma, "To the land or to the sea: diet and mobility in Early Medieval Frisia," *Journal of Island and Coastal Archaeology*, vol. 8, no. 2, pp. 255–277, 2013.

[107] J. E. Ericson, "Strontium isotope characterization in the study of prehistoric human ecology," *Journal of Human Evolution*, vol. 14, no. 5, pp. 503–514, 1985.

[108] S. Hillson, *Dental Anthropology*, Cambridge University Press, Cambridge, UK, 1996.

[109] J. E. Ericson, "Some problems and potentials of strontium isotope analysis for human and animal ecology," in *Stable Isotopes in Ecological Research*, pp. 252–259, Springer, New York, NY, USA, 1989.

[110] J. C. Sealy, N. J. van der Merwe, A. Sillen, F. J. Kruger, and H. W. Krueger, "87Sr86Sr as a dietary indicator in modern and archaeological bone," *Journal of Archaeological Science*, vol. 18, no. 3, pp. 399–416, 1991.

[111] B. K. Nelson, M. J. Deniro, M. Schoeninger, D. J. De Paolo, and P. E. Hare, "Effects of diagenesis on strontium, carbon, nitrogen and oxygen concentration and isotopic composition of bone," *Geochimica et Cosmochimica Acta*, vol. 50, no. 9, pp. 1941–1949, 1986.

[112] P. Budda, B. L. J. Montgomery, P. Rainbird, R. G. Thomas, and S. M. Young, "Pb and Sr isotope composition of human dental enamel: an indicator of Pacific Islander population dynamics," in *Le Pacifique de 5000 à 2000 avant le présent: suppléments à l'histoire d'une colonisation = The Pacific from 5000 to 2000 BP: Colonisation and Transformations*, G. Jean-Christophe and I. Lilley, Eds., Institut de recherche pour le développement, Marseille, France, 1999.

[113] M. Sponheimer and J. A. Lee-Thorp, "Enamel diagenesis at South African Australopith sites: implications for paleoecological reconstruction with trace elements," *Geochimica et Cosmochimica Acta*, vol. 70, no. 7, pp. 1644–1654, 2006.

[114] C. Hänni, V. Laudet, D. Stehelin, and P. Taberlet, "Tracking the origins of the cave bear (*Ursus spelaeus*) by mitochondrial DNA sequencing," *Proceedings of the National Academy of Sciences*, vol. 91, no. 25, pp. 12336–12340, 1994.

[115] P. Argenti and P. P. Mazza, "Mortality analysis of the Late Pleistocene bears from Grotta Lattaia, central Italy," *Journal of Archaeological Science*, vol. 33, no. 11, pp. 1552–1558, 2006.

[116] I. Martini, M. Coltorti, P. P. Mazza, M. Rustioni, and F. Sandrelli, "The latest *Ursus spelaeus* in Italy, a new contribution to the extinction chronology of the cave bear," *Quaternary Research*, vol. 81, no. 1, pp. 117–124, 2014.

[117] H. Bocherens, M. Fizet, and A. Mariotti, "Diet, physiology and ecology of fossil mammals as inferred from stable carbon and nitrogen isotope biogeochemistry: implications for Pleistocene bears," *Palaeogeography, Palaeoclimatology, Palaeoecology*, vol. 107, no. 3-4, pp. 213–225, 1994.

[118] H. Bocherens, D. Billiou, M. Patou-Mathis, D. Bonjean, M. Otte, and A. Mariotti, "Paleobiological implications of the isotopic signatures (^{13}C, ^{15}N) of fossil mammal collagen in Scladina Cave (Sclayn, Belgium)," *Quaternary Research*, vol. 48, no. 3, pp. 370–380, 1997.

[119] H. Bocherens, M. Stiller, K. A. Hobson et al., "Niche partitioning between two sympatric genetically distinct cave bears (*Ursus spelaeus* and *Ursus ingressus*) and brown bear (*Ursus arctos*) from Austria: isotopic evidence from fossil bones," *Quaternary International*, vol. 245, no. 2, pp. 238–248, 2011.

[120] D. Fernández-Mosquera, M. Vila-Taboada, and A. Grandal-d'Anglade, "Stable isotopes data ($\delta^{13}C$, $\delta^{15}N$) from the cave bear (*Ursus spelaeus*): a new approach to its palaeoenvironment and dormancy," *Proceedings of the Royal Society of London B: Biological Sciences*, vol. 268, no. 1472, pp. 1159–1164, 2001.

[121] M. P. Richards, M. Pacher, M. Stiller et al., "Isotopic evidence for omnivory among European cave bears: late Pleistocene *Ursus spelaeus* from the Peştera cu Oase, Romania," *Proceedings of the National Academy of Sciences*, vol. 105, no. 2, pp. 600–604, 2008.

[122] Z. Nerudová, M. Nývltová Fišáková, and J. Míková, "Palaeoenvironmental analyses of animal remains from the Kůlna Cave (Moravian Karst, Czech Republic)," *Quartär*, vol. 61, 2014.

[123] O. Loreille, L. Orlando, M. Patou-Mathis, M. Philippe, P. Taberlet, and C. Hänni, "Ancient DNA analysis reveals divergence of the cave bear, *Ursus* spelaeus, and brown bear, Ursus arctos, lineages," *Current Biology*, vol. 11, no. 3, pp. 200–203, 2001.

[124] L. Orlando, D. Bonjean, H. Bocherens et al., "Ancient DNA and the population genetics of cave bears (*Ursus spelaeus*) through space and time," *Molecular Biology and Evolution*, vol. 19, no. 11, pp. 1920–1933, 2002.

[125] M. Pacher and A. J. Stuart, "Extinction chronology and palaeobiology of the cave bear (*Ursus spelaeus*)," *Boreas*, vol. 38, no. 2, pp. 189–206, 2009.

[126] A. Berton, M. Bonato, A. Borsato et al., "Nuove datazioni radiometriche con il metodo U/Th sulle formazioni stalagmitiche di Grotta all'Onda," *Rivista di Scienze Preistoriche*, vol. 53, pp. 241–256, 2003.

[127] G. Molara, "Resti faunistici provenienti dai livelli del Pleistocene superior di Grotta all'Onda (Camaiore, Lucca)," in *Atti del 6° Convegno Nazionale di Archeozoologia*, pp. 57–62, Centro visitatori del Parco dell'Orecchiella, Lucca, Italy, 2009.

[128] T. Adani, *Applicazioni delle sistematiche geochimiche ed isotopiche a reperti fossili Quaternari*, M.S. thesis, Earth Sciences Department, Università degli Studi di Firenze, 2013.

[129] G. Cortecci and L. Lupi, "Carbon, oxygen and strontium isotope geochemistry of carbonates rocks from the Tuscan Nappe, Italy," *Mineral Petrol Acta*, vol. 37, pp. 63–80, 1994.